29454 DUP

IGM88AP-000-776-G
CNRC 29454

EFFECT OF DEFORMATION ON FERRITE NUCLEATION AND GROWTH IN A PLAIN CARBON AND TWO MICROALLOYED STEELS

E. Essadiqi* and J.J. Jonas
Department of Metallurgical Engineering
McGill University
3450 University Street, Montreal, Canada H3A 2A7

ABSTRACT

Isothermal compression tests were carried out on a plain C, and on a Mo as well as a Mo-Nb-V microalloyed steel in order to study the effect of austenite deformation on the ferrite nucleation and growth rates. The nucleation rate increases with deformation and the degree of supersaturation, Ae_3-T; it appears to be reduced by the substitutional elements Mo, Nb and V through reduction of the austenite grain boundary energy. The growth rate increases with the degree of supersaturation and is also reduced by these elements, apparently through the solute drag-like effect. Under static conditions, increasing the prestraining strain rate increases the nucleation rate but this increase is small compared to the effect of concurrent deformation. The growth rate under static conditions decreases as the deformation or the strain rate is increased.

*Now at the Industrial Materials Research Institute
75, boul. De Mortagne, Boucherville, Quebec J4B 6Y4

EFFECT OF DEFORMATION ON FERRITE NUCLEATION AND GROWTH IN A PLAIN CARBON AND TWO MICROALLOYED STEELS

I INTRODUCTION

The essence of the controlled rolling of HSLA steels is to produce a fine ferrite grain size. This is normally achieved by finish rolling in the no-recrystallization temperature range. However, still further refinement of the ferrite grain size can be produced by applying the last few passes at temperatures below the Ar_3, i.e. in the austenite plus ferrite, intercritical range. The formation of polygonal ferrite from deformed austenite is controlled by both nucleation and growth. However, the nucleation rate is more effective than the growth rate for controlling the ferrite grain size. It is therefore of considerable interest to characterize the effect of deformation on the nucleation process.

The present study was undertaken with the further objective of determining the effect of the microalloying elements Mo, Nb and V on ferrite nucleation and growth in a plain C and two microalloyed steels. The experiments were first carried out under dynamic conditions in order to study the effect of strain and strain rate on the kinetics of nucleation and growth during deformation. A second set was carried out under static conditions with different prestrains and prestraining strain rates. The approach of DeHoff (1) was used to determine quantitatively the nucleation and growth rates. This method is based on the assumption of a general two-parameter particle size distribution, and relies on the estimation of these two parameters from three counting measurements carried out on metallographic sections of the structure. These counting measurements are used to determine: (i) the total surface area, (ii) the volume fraction, and (iii) the number of ferrite 'particles' observed per unit area.

II MATERIALS AND EXPERIMENTAL PROCEDURE

The chemical compositions of the three steels studied are listed in Table I. The procedure used to prepare and deform the specimens has been described in an earlier paper (2). After straining and quenching, the test samples were sectioned parallel to the deformation axis and polished for optical examination. Two different etchants were used: the polished samples were first etched with a 3% nital solution for 10 to 15 seconds in order to reveal the ferrite grain boundaries; they were further etched with a solution consisting of 10g of $Na_2S_2O_5$ in 100 ml of H_2O for 5 to 10 s (3) in order to enhance the contrast between the ferrite and martensite. The volume fraction of ferrite was assessed using standard point counting procedures (4).

Ferrite Grain Size Distribution

The particle (ferrite) size distributions were determined from simple counting measurements on plane sections (1). This technique involves the following quantities: N_A = the number of particle sections observed in a unit area of microsection, N_L = the number of particle intercepts encountered by a unit length of random test line, and P_P = the fraction of points in a randomly placed grid of test points which lies in the phase of interest (ferrite) in the microstructure.

In the general case of partial contiguity, N_L is given by:

$$N_L = \frac{2N_{L\alpha\alpha} + N_{L\alpha\gamma}}{L_T} \qquad (1)$$

where $N_{L\alpha\gamma}$ is the number of intercepts of the sampling line with the interface between the matrix and the phase of interest α, and $N_{L\alpha\alpha}$ is the corresponding measurement for the interface between two particles of the same phase α, and L_T is the total length of the sampling line.

$N_{L\alpha\alpha}$ and $N_{L\alpha\gamma}$ were evaluated from the number of intercepts that 8 parallel lines each 73 mm in length made, respectively, with the α/α and α/γ interfaces. Each sample was analyzed by using 20 different fields, in which the parallel lines were randomly oriented. The quantity N_A was determined by taking the average of 10 measurements for each sample. Furthermore, each measurement was carried out within an area 71 x 71 mm^2.

This method was applied to the log-normal distribution (1), which has been justified empirically (5-7), and is defined by:

$$g(D) = \left[1/sD\sqrt{2\pi}\right] exp\left(- \frac{1}{2}\left[\frac{\ell nD - m}{s}\right]^2\right) \tag{2}$$

$$m = \ell n\, \mu_g \tag{3}$$

$$s = \ell n\, \sigma_g \tag{4}$$

Here D is the ferrite grain size, μ_g is the geometric mean diameter, and σ_g is the geometric standard deviation of the distribution.

This distribution is completely defined by the two parameters m and s, which can be evaluated from the quantitative metallography measurements N_A, N_L and P_p. The calculation of the mean ferrite grain size $D_\alpha(\mu_g)$ and the total number of ferrite grains per unit volume N_V was done with the aid of the following relations:

$$D_\alpha = K_D \cdot \frac{N_L^4}{N_A^{5/2} \cdot P_P^{3/2}} \tag{5}$$

$$N_V = K_V \cdot \frac{N_A^3 \cdot P_P}{N_L^3} \tag{6}$$

where K_D and K_V are constants depending on the shape factors of the particles of ferrite, which were assumed to be spherical in this case.

III RESULTS

A. Nucleation Rate in the Dynamic Austenite-to-Ferrite Transformation

By employing the relations developed above, the total number of particles per unit volume N_V, and the mean ferrite grain size D_α were calculated for the three steels under the various experimental conditions. This was done at temperatures of 790 to 820, 790 to 840 and 800 to 880°C for the plain C, Mo and Mo-Nb-V steels, respectively, and for times up to 1000 s. The results obtained are presented in the form of log-normal distributions in Figs. 1a, b and c for the plain C and Mo steels at 790°C and the Mo-Nb-V steel at 800°C, respectively. The mean diameter is identified by a vertical line in each distribution.

The total number of ferrite particles N_v per unit volume (mm^{-3}) are plotted versus time (i.e. deformation) at selected temperatures in Figs. 2a, b and c for the plain C, Mo and Mo-Nb-V steels, respectively. N_v increases very rapidly at the beginning of the austenite-to-ferrite transformation (i.e. at times below 100 s) and then the rate of increase is reduced. At very long times, the curves all display asymptotic behavior due to saturation of the active sites for ferrite nucleation. The nucleation start time decreases as the temperature is decreased. The nucleation rate is given by (8):

$$J_v = \frac{1}{U(t)} \cdot \frac{dN_v}{dt} \quad nuclei/unit\ volume\ of\ untransformed\ austenite/s \tag{7}$$

Here N_v is the number of ferrite particles per unit volume, and U(t) is the volume fraction of untransformed austenite. The nucleation rate at grain boundaries is properly expressed as the number of nuclei per unit *unreacted* austenite grain boundary area per unit time (8-10). For this purpose, Mazanec and Cadek (8) used the Saltykov relation:

$$J_s = \frac{1}{U(t)} \cdot \frac{dN_v}{dt} \cdot \frac{1}{S_\gamma} \tag{8}$$

where S_γ is the austenite grain boundary area per unit volume. This nucleation rate is austenite grain size independent, which is useful for studying the effect of other parameters, such as the influence of alloying elements on the nucleation rate. S_γ was calculated from the following relation (11):

$$S_\gamma = \frac{2}{D_\gamma} \tag{9}$$

where D_γ is the austenite grain size. In this study, $D\gamma \simeq 25\ \mu m$ for the three steels.

From the slopes dN_v/dt, of the above curves, the nucleation rates (expressed in terms of the number of nuclei per unit unreacted grain boundary area per s) were determined using relation (8). These rates are shown in Figs. 3a, b and c for the plain C, Mo and Mo-Nb-V steels, respectively.

In all cases, the nucleation rate increases very quickly in the early stage of transformation, reaches a maximum value, and then decreases with time. These maxima, which are tabulated in Table II for the three steels, decrease as the temperature is increased (i.e. as the driving force for transformation is decreased). Also, the time corresponding to the maximum increases with temperature (i.e. as the driving force is reduced).

The dependence of the maximum nucleation rate on temperature for the three steels is shown in Fig. 4. In the temperature range of this study, the maximum nucleation rate decreases as the temperature is increased. This is due to the concurrent decrease in the driving force, as mentioned above. At high temperatures, above 810°C, the maxima for the Mo-Nb-V and Mo steels are higher than those pertaining to the plain C steel. At lower temperatures, the order is reversed.

B. Nucleation Rates in the Static Austenite-to-Ferrite Transformation

The evolution of the number of nuclei per unit volume versus time in the Mo steel at 800°C is shown in Fig. 5 for predeformations of 0.0, 0.10, and 0.20, as well as for two strain rates (7.4×10^{-2} and 7.4×10^{-1} s^{-1}) at the latter predeformation. The evolution of N_v in the dynamic case at the same temperature and for the same steel

is also displayed for comparison purposes. It is evident that N_v increases with predeformation and strain rate. It should also be noted that the N_v's for all the static cases are very low with respect to the dynamic N_v's. The slopes of these curves, dN_v/dt, which are related to the nucleation rates by relation (8), are illustrated in Fig. 6. As the predeformation and strain rate are increased, the nucleation start time is reduced and the nucleation rate is increased. The maximum nucleation rates are tabulated in Table III.

It is apparent that J_{max} increases with predeformation; increasing the strain rate is also effective in accelerating the nucleation rate. In the dynamic case, the maximum is about 30 times greater than in the static case, Table III.

C. Growth Rate in the Dynamic Case

The ferrite growth rate in the current plain C, Mo and Mo-Nb-V steels is presented below in terms of the evolution of the mean diameter D_α of ferrite formed during the dynamic austenite-to-ferrite transformation, as determined by relation (5). The evolution of D_α versus $\sqrt{t\text{-}t_0}$ (t_0 is the time corresponding to the formation of 5% ferrite) is shown in Figs. 7a, b and c for the plain C, Mo and Mo-Nb-V steels, respectively. In all cases, straight line fits are observed, and growth therefore obeys the parabolic law, in accordance with the relationship:

$$D_\alpha = a\sqrt{t - t_o} \qquad (10)$$

where a is the parabolic growth rate parameter. It is given by the slopes of the lines in the above figures. The values of this parameter for the three steels at the different experimental temperatures are listed in Table IV and plotted in Fig. 8. The parameter a increases with decreasing temperature (i.e. increasing

supersaturation). At a given temperature, the growth rate parameter for the Mo-Nb-V steel is higher than that for the Mo steel, which is, in turn, higher than that for the plain C steel. This is because, at a given temperature, the three steels have different levels of supersaturation, which increase with the total content of the α stabilizing elements Mo, Nb and V. The latter, in turn, leads to an increase in the Ae_3 temperature.

D. Growth Rate of the Ferrite in the Static Case

The evolution of the mean grain size of the ferrite formed statically in the Mo steel at 800°C is shown in Fig. 9. The effect of predeformations of 0.1 at 7.4×10^{-2} s^{-1} and 0.2 at strain rates of 7.4×10^{-1} and 7.4×10^{-2} s^{-1} is illustrated and compared with the 'no prestrain' ($\varepsilon = 0.0$) behaviour. This evolution with respect to $\sqrt{t - t_o}$ demonstrates that the rates follow the parabolic growth law. As the predeformation or the strain rate is increased, the slope of the line decreases, as does the resultant ferrite grain size.

IV DISCUSSION

A. Comparison Between the Experimental Results and the Predictions of the Classical Nucleation Theories

The shape of the critical nucleus is important in the evaluation of the nucleation rate by the classical theory of nucleation (12-14). Numerous models based on different shapes of the critical nucleus have been applied to experimentally observed ferrite nucleation rates in Fe-C and Fe-C-X (9, 10, 15, 16) as well as for

proeutectoid α in Ti-X (17, 18). The nucleus model based on a spherical cap was found to be invalid for the proeutectoid ferrite reaction (9, 17). An alternative approach using the traditional disk shaped pillbox, but with all of its interfaces assumed to be partially or fully coherent, Fig. 10, and thus to have a lower energy, has been applied successfully (15-19).

In classical nucleation theory, the time dependent nucleation rate J^* was expressed as (13):

$$J^* = Z\beta^* N \cdot \exp\left(-\frac{\Delta G^*}{kT}\right)\exp\left(-\frac{\tau}{t}\right) \tag{11}$$

Here J^* is the nucleation rate, Z is the Zeldovich non-equilibrium factor, β^* the frequency factor, N the density of sites available for nucleation, ΔG^* the Gibbs free energy of activation for nucleation, τ the incubation time, t the isothermal reaction time and kT has its usual meaning.

By dropping the last term of the above equation, the steady state nucleation rate J^*_s in the pillbox model of Fig. 10 can be restated as (9, 16):

$$J^*_s = \frac{2ND X_\gamma V_\alpha \varepsilon^{1/2}}{a^4(3kT)^{1/2}} \cdot \exp\left(-\frac{4\pi(\sigma^e_{\alpha\gamma})^2\varepsilon}{\phi^2 kT}\right) \tag{12}$$

Here $\varepsilon = \sigma_{\alpha\gamma}{}^{e} + \sigma_{\alpha\gamma}{}^{cb} - \sigma_{\gamma\gamma}$, D is the diffusivity of the solute, X_γ the atom fraction of carbon in the matrix, V_α the molar volume of ferrite, a the average lattice parameter of the two phases, ϕ the sum of (i) the volume free energy change ΔG_v associated with nucleation, (ii) the stored energy ΔG_d associated with the dislocations created by the deformation and (iii) the volume strain energy ΔG_ε.

The radius of the critical nucleus, r^*, and the critical nucleus height, h^*, were defined as follows:

$$r^* = - \frac{2\sigma^e_{\alpha\gamma}}{\phi} \tag{13}$$

$$h^* = - \frac{2\varepsilon}{\phi} \tag{14}$$

This model, which was developed for *static* transformations in high purity Fe-C and Fe-C-X alloys (where X = Co, Mn, Mo and Ni), (9, 10, 15, 16), was applied to the present dynamic results. In particular, the steady state nucleation rate J^*_s was predicted using this formalism and the estimates correspond to the experimental J^*_{max} values associated with each temperature in the three steels.

For this purpose, equation (12) was used. The volume free energy change ΔG_v was taken from the expression given by Aaronson, Kinsman and Russell (20) for a binary system:

$$\Delta G_v = - \frac{RT}{V_\alpha} \ell n \frac{1 - X_\gamma}{1 - X^{\alpha\gamma}_\gamma} \tag{15}$$

Here $X^{\alpha\gamma}_\gamma$ is the atom fraction of carbon in the austenite at the $(\alpha + \gamma)/\gamma$ phase boundary. Their values were calculated for the three steels at different temperatures by using a thermodynamic model (21, 22). The values of ΔG_v are given in Table V. The dislocations created by the deformation increase the energy of the austenite, particularly near grain boundaries. The stored energy ΔG_d of deformation is about (23):

$$\Delta G_d = - \tau\rho \tag{16}$$

Here τ is the dislocation line energy and ρ the dislocation density. The former is in turn defined by:

$$\tau = \frac{\mu b^2}{2} \tag{17}$$

so that $\tau = 2.3 \times 10^{-9}$ J/m. Finally, for $\rho = 10^{15}/m^2$ (23) ΔG_d is found to be approximately -2×10^6 J/m^3. In the current study, where the driving force ΔG_v increases from zero to about -10×10^6 J/m^3 in the temperature range studied, the stored energy of deformation cannot be neglected. As an approximation, the value of ΔG_d was added to the chemical driving force ΔG_v in the calculation of the nucleation rate. The strain energy ΔG_ε was taken as 0 (this assumption being reasonable since the free volume in the grain boundary can accommodate the volume increase due to the formation of ferrite). Thus

$$\phi = \Delta G_v + \Delta G_d \tag{18}$$

ε was calculated from relation (14) by setting h^* equal to the unit cell of ferrite.

The values of the diffusivity D of carbon in austenite were calculated from the following relation (24):

$$D_c^\gamma = 0.5 \exp(-30 X_\gamma) \exp(-Q_D(X_\gamma)/RT)\ cm^2/s \tag{19}$$

where

$$Q_D(X_\gamma) = 38300 - 1.9 \times 10^5 X_\gamma + 5.5 \times 10^5 X_\gamma^2\ cal/mole \tag{20}$$

The lattice parameters a_α and a_γ for ferrite and austenite were calculated from the molar volumes of ferrite and austenite given by Kaufman (25):

$$V_\alpha(T) = 6.991\,(1 + 4.68 \times 10^{-5} T)\ cm^3/mole \tag{21}$$

$$V_\gamma(T) = 6.679\,(1 + 7.89 \times 10^{-5} T)\ cm^3/mole \tag{22}$$

where T is in °K.

Thus

$$a_\alpha = \left(\frac{2\,V_\alpha}{N_o}\right)^{1/3} \tag{23}$$

and

$$a_\gamma = \left(\frac{4\,V_\gamma}{N_o}\right)^{1/3} \tag{24}$$

$N_0 = 6.022 \times 10^{23}$/mole is Avogadro's number.

There are no experimental values of the energies of even disordered austenite-ferrite boundaries available in the alloys of interest. However, the edge energy, $\sigma^e_{\alpha\gamma}$, can be estimated as $\simeq$ 20 mJ/m^2 (9, 10, 19). This appears to be a reasonable value for the energy of a fully coherent α/γ interface. The density of nucleation sites N was then taken as 10^5/cm^2, i.e. much below its 'normal' value of 10^{15}/cm^2, because of the large reduction expected when a special orientation relationship applies between the austenite and ferrite (10). The nucleation rates calculated in this way are given in Table VI for the plain C, Mo and Mo-Nb-V steels, respectively, and compared with the experimental values. Here the rates are given per unit unreacted austenite grain boundary area per unit time. The calculated and measured nucleation rates for the plain C steel are in agreement within an order of magnitude. For the Mo and Mo-Nb-V steels, the agreement is less good, but is within two orders of magnitude. Better agreement is consistent with a still lower value for N than assumed above, and lower assumed values of $\sigma^e_{\alpha\gamma}$.

The discrepancies may also be associated with a number of other factors: i) the driving force, which was approximated by the relation for binary alloys, and which affects the nucleation rate through the activation energy $\Delta G^* = K/\phi^2$ in an exponential manner: ii) the effect of deformation on the driving force, which is not

well known; and iii) inaccuracies in the simple models for ferrite nucleation at austenite grain boundaries (10, 19), a subject which requires more theoretical study.

B. The Effect of Deformation on Nucleation Rate

It is well known that the deformation of austenite increases the nucleation rate of ferrite and moves the TTT curves to shorter times (2, 26-32). It has also been reported by Desalos et al. (32) that, after the controlled rolling of low alloy steels, there is an increase in the ferrite nucleus density in deformed austenite. Several mechanisms by which deformation increases the nucleation rate of ferrite have been proposed. Sandberg and Roberts (23, 29), have suggested that the prolific nucleation of ferrite in deformed austenite is associated with the bulges formed by local austenite grain boundary migration. Amin and Pickering (30) have proposed that the formation of subgrains near deformed austenite grain boundaries increases the nucleation rate of ferrite. Umemoto and Tamura (31) have suggested that the strain energy of the dislocations stored in deformed austenite favors ferrite nucleation within deformed austenite.

In the present study, the maximum nucleation rate of ferrite for the three steels increased as the temperature was decreased, Fig. 4. This is due to the concurrent increase in the driving force for transformation. As the temperature is decreased, the chemical driving force increases in absolute value. The dislocation density created by the deformation also increases, as does the stored energy ΔG_d of the austenite. At a given temperature, increasing the strain rate is also effective in accelerating nucleation. In the case of the Mo steel at 800°C, by increasing the strain

rate from 7.4×10^{-4} to 7.4×10^{-1} s^{-1}, the nucleation rate was increased by about three orders of magnitude. Increasing the strain rate also increases the homogeneity of the ferrite microstructure, leading to very fine grain sizes ($\approx$ 2 μm) (2).

C. Nucleation Rate during Static Transformation

The ferrite nucleation rate during static transformation was increased by prestraining, as can be seen from Table III for the Mo steel at 800°C. It was also accelerated by increasing the strain rate. However, these increases are small compared to the effect of *concurrent* deformation. For instance, the nucleation rate in the dynamic case for the Mo steel at 800°C and a strain rate of 7.4×10^{-4} s^{-1} is about 30 times greater than during static transformation without predeformation, see Table III. Increasing the strain rate increases this ratio by the same order of magnitude.

D. The Effect of Alloying Elements on the Nucleation Rate

As illustrated in Fig. 4, Mo, Nb and V increase the nucleation rate of ferrite at high temperatures because they raise the Ae_3 temperature and thus the driving force $|\Delta G_v|$. Above about 810°C, J_{max} is higher in the ternary than in the Mo steel, and in the latter than in the plain C steel. At lower temperatures, the order is reversed, illustrating the reduction in nucleation rate caused by these elements. Similar results were reported for the effect of Mo in Fe-C-Mo (16). The maximum nucleation rates at different temperatures for the dynamic austenite-to-ferrite transformation are shown in Fig. 11, plotted with respect to $\Delta T = Ae_3 - T$. (Note

that the three steels have different γ-to-α transformation temperatures). For a given amount of supercooling ΔT, the maximum nucleation rate is higher in the plain C than in the Mo steel, and in the latter than in the Mo-Nb-V steel. It is therefore apparent that the nucleation rate is reduced by the presence of the microalloying elements Mo, Nb and V.

The effect of alloying elements on the ferrite nucleation rate described above is consistent with several recent literature results. It was reported by Aaronson et al. (10, 16, 33) that Mo retards the nucleation rate of ferrite. This effect was explained in terms of the segregation of Mo to the austenite grain boundaries, which lowers the austenite grain boundary energy and thus increases the net interfacial free energy necessary to form a ferrite nucleus. Ouchi et al. (27) noted that Nb retards the austenite to ferrite transformation in a similar manner . Although the influence of V has not been studied in detail, it may act as Mo and Nb in retarding the nucleation rate of ferrite.

E. Growth Rate in the Dynamic Case: (i) Effect of Mo, Nb and V on the Growth Rate of Ferrite

The influence of Mo, Nb and V in solution in the austenite of the present steels on the growth rate of polygonal ferrite is shown in Fig. 12. This diagram illustrates the dependence of the parabolic growth rate parameter on the degree of undercooling (Ae_3 - T). At a given undercooling; ΔT, the rate constant for the plain C steel is higher than that for the Mo or the Mo-Nb-V steel. This difference increases as the temperature is decreased. The Mo growth rate parameter is distinctly higher than

that of the Mo-Nb-V steel at relatively high undercooling; but at low supersaturation, the α's are similar. Thus it seems that an addition of 0.3% of Mo is more effective than that of 0.10% V or of 0.035 (wt)% Nb in reducing the growth rate of ferrite. Although the effects of adding these elements are not "linear" in nature, nor is their influence additive, the addition of the Mo (0.17 atomic %) has a retarding effect about an order of magnitude greater than that of the V (0.13 atomic %) and the Nb (0.02 atomic %). This suggests that Mo is about ten times as effective as V on an equal atom fraction basis; the Nb level is too low, on the other hand, for their relative 'strengths' to be assessed in this way.

(ii) Solute Drag-Like Effect (SDLE)

Two kinetic effects of the substitutional alloying elements on the ferrite growth rate have been recognized. One is the solute drag-like effect. The second is interphase boundary carbide precipitation (34, 35). Some substitutional alloying elements influence austenite-ferrite interface motion through a solute drag-like effect, SDLE (36-39). The existence of this effect was suggested by Kinsman and Aaronson (39), as well as by Hillert (37). Recently, suggestions have been made that the substitutional elements Cr, Mn, Mo, Ti and V affect the growth rate by SDLE (10, 40-42). In this approach, an alloying element that has an appreciable size misfit with respect to the Fe atom (austenite or ferrite) segregates to the disordered austenite/ferrite interface during growth and attracts carbon atoms. If the alloying element *decreases* the activity of carbon in austenite, it tends to collect carbon atoms, and so to reduce the concentration of carbon in the austenite in regions remote from itself. As the carbon concentration at the boundary is increased in this way, the

growth kinetics are retarded. Conversely, if the alloying element *increases* carbon activity in austenite and still segregates to the disordered α/γ interface because of the size misfit, it tends to 'scavenge' the boundary of carbon, leading to an inverse SDLE. The growth rate can be expected to be increased by the addition of such elements. Indeed, Si and Al, which increase the activity of carbon, were found to increase the growth rate of ferrite (40, 38), whereas Mn, Cr and Mo (38, 39), which decrease the activity of carbon, reduce the growth rate, presumably by the SDLE.

In this respect, Mo is more effective than Cr, especially at low temperatures; this is consistent with the larger misfit of Mo (10). V, which is a strong carbide former, exhibits a moderate size misfit with respect to Fe, and also decreases carbon activity appreciably in austenite. However, its effect in reducing the growth rate by SDLE is limited by its small solubility in austenite (41, 42). This explains why V shifts the TTT curve for the initiation of the proeutectoid ferrite reaction so little compared with Cr and Mo. The SDLE can also be diminished by the occurrence of interphase boundary carbide precipitation (42). The V carbonitride precipitation observed in Mo-Nb-V steel (22) takes place in sub-boundaries in ferrite, subsequent to the γ-α transformation, suggesting that there is no correlation between such precipitation and the growth rate of ferrite.

Similar considerations are involved in the addition of Nb to austenite; it exhibits a larger size misfit than Mo, Cr or V, and also reduces the activity of C. In fact, the Wagner interaction parameter ε^{C}_{Nb} for Nb is considerably more negative than that of Mo, Cr or V (22), see Table VII. Thus the SDLE produced by a given atom fraction of Nb is expected to be very strong. Nevertheless, in the present Mo-Nb-V steel, the Nb concentration is very low (0.02 at. pct), and is an order of

magnitude lower than that of Mo (0.17 at. pct). The Nb concentration (in solution) may be even lower than that mentioned above because undissolved Nb(C,N) precipitates may be present in the steel. As indicated earlier, this can explain why the growth rate parameters for the Mo and Mo-Nb-V steels differ by one order of magnitude less than the rate parameters for the Mo and plain C steels.

F. Effect of Deformation on the Growth Rate of Ferrite

The dependence of the parabolic growth rate parameter (slope of the line) on the predeformation is shown in Fig. 13. Only one point is illustrated for the strain rate of 7.4×10^{-1} s^{-1} corresponding to a predeformation of $\varepsilon = 0.2$. The horizontal line corresponds to the dynamic case. It is evident that the growth rate parameter decreases as the predeformation increases. This decrease may be related to the increase in the nucleation rate with prestrain, i.e. in the number of nuclei per unit unreacted austenite grain boundary area. The high nucleus density, in turn, can lead to a size reduction by impingement of the growing ferrite grains. This can arise because the growth rate parameter was calculated from the evolution of the mean diameter of ferrite (rather than from the largest observable grain, as is sometimes done).

CONCLUSIONS

As a result of this study, the following conclusions were reached.

1. Under dynamic transformation conditions, the ferrite nucleation rate increases with the degree of supersaturation, Ae_3 - T; it is reduced by the presence of the microalloying elements Mo, Nb and V. This reduction seems to be related to the lowering of the boundary energy $\sigma_{\gamma\gamma}$ by the segregation of Mo, Nb and V to the γ/γ grain boundaries. The results indicate that 0.3% Mo is more effective in reducing the nucleation rate than the combination of 0.035% Nb and 0.11% V.

2. In the static case, the nucleation rate is increased by prestraining, but this increase is small compared to the effect of concurrent deformation. In the Mo steel at 800°C, the maximum nucleation rate is about 30 times greater in the dynamic than in the static case. Increasing the strain rate is also effective in accelerating the nucleation rate.

3. The measured maximum nucleation rates in the dynamic case were compared to ones calculated from the pillbox model; the agreement observed is reasonable: i.e. within an order of magnitude for the plain C steel and two orders of magnitude for the Mo and Mo-Nb-V steels. Better agreement can be achieved if lower values are employed for the nucleus site density and if a lower value of the interface edge energy $\sigma^{e}_{\alpha\gamma}$ is assumed.

4. The dynamic ferrite growth rate in the three steels follows a parabolic law. In all cases, the growth rate parameter α increases with decreasing temperature (i.e. increasing supersaturation). At a given temperature, the parameter α for the Mo-Nb-V steel is higher than that for the Mo steel, which is in turn higher than that for the plain C steel. This is due to the different levels of supersaturation which increase with the total content of the α stabilizing elements Mo, Nb and V.

5. At a given undercooling $\Delta T = Ae_3 - T$, the rate constant for the plain C steel is higher than that for the Mo or for the Mo-Nb-V steel. This difference increases as the temperature is decreased. The Mo, which exhibits a large misfit and decreases the activity of C, is more effective than V in reducing the ferrite growth rate, presumably by the solute drag-like effect (SDLE). V, which has a moderate size misfit, is less effective in reducing the α parameter by SDLE, perhaps because of its low solubility in austenite. Nb, despite its large size misfit, only has a small effect on the ferrite growth rate, probably as a result of its very low concentration (0.02 atomic pct.).

6. The growth rate parameter under static conditions for the Mo steel at 800°C decreases as the predeformation or the strain rate is increased.

ACKNOWLEDGEMENTS

The authors acknowledge with gratitude the assistance received from Dr. G.E. Ruddle of CANMET with respect to the provision of experimental materials. They are also thankful to CANMET for financial support, as well as to the Natural

Sciences and Engineering Research Council of Canada, the Quebec Ministry of Education (FCAR program), and the Canadian Steel Industry Research Association.

REFERENCES

1. R.T. DeHoff: Trans. AIME, 1965, 233, pp. 25-29.

2. E. Essadiqi and J.J. Jonas: Metall. Trans. 1988, 19A, pp. 417-426.

3. A.M. Marder and A.O. Benscoter: Metallography, 1982, 15, pp. 73-85.

4. H. Abrams: "Stereology and Quantitative Metallography", ASTM STP 504, American Society for Testing and Materials, 1972, pp. 138-182.

5. P. Feltham: Acta Metall., 1957, 5, pp. 97-105.

6. M. Hillert: Acta Metall., 1965, 13, pp. 227-238.

7. J.E. Hilliard: Trans. AIME, 1968, 242, pp. 1373-1380.

8. K. Mazanec and J. Cadek: Mem. Sci. Rev. Metall., 1958, 55, pp. 501-512.

9. W.F. Lange III: "Ph.D Thesis, Michigan Technological University, Houghton, MI, 1979.

10. W.T. Reynolds, Jr., M. Enomoto and H.I. Aaronson: "Phase Transformations in Ferrous Alloys", A.R. Marder and J.I. Goldstein, Eds., TMS-AIME, Warrendale, PA, 1984, pp. 155-200.

11. I. Kozasu, C. Ouchi, T. Sampei and T. Okita: "Microalloying 75", Union Carbide Corporation, New York, 1975, pp. 120-135.

12. K.C. Russell: Advances in Colloid and Interface Science, 1980, 13, pp. 205.

13. H.I. Aaronson and J.K. Lee: "Lectures on the Theory of Phase Transformations", H.I. Aaronson, Ed., 1982, pp. 83-115.

14. W.C. Johnson, C.L. White, P.E. Marth, P.K. Ruf, S.M. Tuominen, K.D. Wade, K.C. Russell and H.I. Aaronson: Metall. Trans., 1975, 6A, pp. 911-919.

15. M. Enomoto, W.F. Lange, III, and H.I. Aaronson: Metall. Trans., 1986, 17A, pp. 1399-1407.

16. M. Enomoto and H.I. Aaronson: Metall. Trans., 1986, 17A, pp. 1385-1397.

17. M.R. Plichta, J.H. Perepezko, H.I. Aaronson and W.F. Lange III: Acta Metall., 1980, 28, pp. 1031-1040.

18. E. Sarath Kumar Menon and H.I. Aaronson: Metall. Trans., 1986, 17A, pp. 1703-1715.

19. H.I. Aaronson and K.C. Russell: "Solid-Solid Phase Transformations"; H.I. Aaronson, Ed., TMS-AIME, Warrendale, PA, 1983, pp. 371-397.

20. H.I. Aaronson, K.R. Kinsman and K.C. Russell: Scripta Metall., 1970, 4, pp. 101-106.

21. K. Hashigushi, J.S. Kirkaldy, T. Fukuzumi and V. Pavaskar: CALPHAD, 1984, 8, pp. 173-186.

22. E. Essadiqi: Ph.D. Thesis, 1986, McGill University, Montreal.

23. A. Sandberg and W. Roberts: "Thermomechanical Processing of Microalloyed Austenite", A.J. DeArdo, G.A. Ratz and P.J. Wray, Eds., TMS-AIME, Warrendale, PA, 1982, pp. 405-431.

24. L. Kaufman, S.V. Radcliffe and M. Cohen: "Decomposition of Austenite by Diffusional Processes", V.F. Zackay and H.I. Aaronson, Eds., Interscience, 1962, pp. 313-352.

25. L. Kaufman, E.V. Clougherty and R.J. Weiss: "Perspectives in Ferrous Metallurgy", Pergamon Press, Oxford, 1985, pp. 181.

26. I. Kozasu, C. Ouchi, T. Sampei and T. Okita: "Microalloying 75", Union Carbide Corporation, New York, 1975, pp. 120-135.

27. C. Ouchi, T. Sampei and I. Kozasu: Trans. ISIJ, 1982, 22, pp. 214-222.

28. H. Inagaki: Trans. ISIJ, 1983, 23, pp. 259-106.

29. W. Roberts, H. Lidefelt and A. Sandberg: "Hot Working and Forming Processes", C.M. Sellars and G.J. Davies, Eds. The Metals Society, London, 1980, pp. 38-42.

30. R.K. Amin and F.B. Pickering: Ref. 29, pp. 377-403.

31. M. Umemoto and I. Tamura: Proc. Conf. on "Microalloyed Steels 35', CSM, Beijing, China, 1985, pp. 373-382.

32. Y. Desalos, A. LeBon and R. Lombry: "Les Traitements Thermomécaniques: Aspects Théoriques et Applications", 24eme colloque de métallurgie, INSTN, Saclay, France, 1981, pp. 137-147.

33. H.I. Aaronson, H.A. Domian and G.M. Pound: Trans. AIME, 1966, 236, pp. 768-780.

34. A.T. Davenport, F.G. Berry and R.W.K. Honeycombe: Metal Sci., 1968, 2, pp. 104-106.

35. J.M. Gray and R.B.G. Yeo: ASM Trans. Quart., 1968, 61, pp. 255.

36. D.E. Coates: Metall. Trans. 1973, 4, pp 2313-2325.

37. M. Hillert: "The Mechanism of Phase Transformation in Crystalline Solids", Inst. of Metals, London, Monograph 1969, 33, pp. 231-247.

38. K.R. Kinsman and H.I. Aaronson: Metall. Trans., 1973 ,4, pp. 959-967.

39. K.R. Kinsman and H.I. Aaronson: "Transformation and Hardenability in Steels", Climax Molybdenum, Co., 1971, pp. 39-53.

40. J.R. Bradley and H.I. Aaronson: Metall. Trans., 1981, 12A, pp. 1729-1741.

41. T. Abe, H.I. Aaronson and G.J. Shiflet: Metall. Trans., 1985, 16A, pp. 521-527.

42. J.R. Bradley, G.J. Shiflet and H.I. Aaronson: Ref. 19, p. 819.

Table I Chemical Compositions (wt%) of the Materials Tested*

Steel	C	Mn	Si	Al	Mo	Nb	V
Plain C	.06	1.42	.24	.025	-	-	-
Mo	.05	1.34	.20	.065	.29	-	-
Mo-Nb-V	.06	1.16	.20	.030	.30	.035	.115

*The nitrogen level was 60 ppm in all three steels.

Table II Maximum Nucleation Rates J^*_{max} Observed in the Three Steels

T°C	J^*_{max} (Nuclei/cm^2/s)		
	Plain C	Mo	Mo-Nb-V
880	-	-	1.65×10^4
860	-	-	3.09×10^4
840	-	3.82×10^4	3.67×10^4
820	3.41×10^4	5.43×10^4	4.61×10^4
800	8.00×10^4	6.31×10^4	5.61×10^4
790	11.50×10^4	6.63×10^4	-

Table III Maximum Static Nucleation Rates for the Mo Steel at 800°C with Different Predeformations

ε	$\dot{\varepsilon}$ s^{-1}	J^*_{max} (nuclei/cm^2/s	J^*_{max} dyn/J^*_{max} stat
0.0	7.4×10^{-2}	2.13×10^3	29.60
0.10	7.4×10^{-2}	3.92×10^3	16.09
0.20	7.4×10^{-2}	5.06×10^3	12.47
0.20	7.4×10^{-1}	7.89×10^3	8.00
dynamic case	7.4×10^{-4}	6.31×10^4	1.00

Table IV Measured Ferrite Growth Rate Parameter α ($\mu m/\sqrt{s}$) for the Plain C, Mo and Mo-Nb-V Steels

Temperature °C	Plain C	Mo	Mo-Nb-V
790	0.20	0.22	-
800	0.15	0.16	0.17
820	0.11	0.12	0.13
840	-	0.10	0.11
860	-	-	0.10
880	-	-	0.09

Table V Estimated Driving Forces Under the Various Experimental Conditions*

T°C	ΔG_v (J/m^3)		
	Plain C	Mo	Mo-Nb-V
880	-	-	-0.574×10^6
860	-	-0.839×10^6	-1.616×10^6
840	-0.618×10^6	-2.145×10^6	-3.283×10^6
820	-2.593×10^6	-4.134×10^6	-5.578×10^6
800	-5.187×10^6	-6.790×10^6	-8.518×10^6
790	-6.742×10^6	-8.370×10^6	-10.525×10^6

*Calculated from the relation $\Delta G_v = -RT/V_\alpha \, \ell n \, (1 - X_\gamma)/1 - X^{\alpha\gamma}_\gamma)$

Table VI Experimental and Calculated Nucleation Rates (Number of Nuclei/cm^2/s) for the Plain C, Mo and Mo-Nb-V Steels

Steel	Temperature °C	J* max exp.	J^*_s calculated
Plain C	820	3.41×10^4	2.07×10^4
	800	8.00×10^4	7.48×10^5
	790	11.50×10^4	22.5×10^5
Mo	840	3.82×10^4	1.05×10^4
	820	5.43×10^4	3.37×10^5
	800	6.31×10^4	2.88×10^6
	790	6.63×10^4	5.98×10^6
Mo-Nb-V	880	1.65×10^4	2.5×10^2
	860	3.09×10^4	3.09×10^3
	840	3.67×10^4	1.40×10^5
	820	4.61×10^4	1.68×10^6
	800	5.61×10^4	7.92×10^6

Table VII The Wagner Interaction Parameter ε_x^c at 800°C in Austenite (19)

Symbol	ε_x^c
Cr	-13.96
Mn	- 4.48
Mo	-12.79
Nb	-61.75
Ni	+ 5.15
Si	+13.78
V	-22.98

FIGURE CAPTIONS

Figure 1a Evolution of the ferrite grain size log-normal distribution for the plain C steel at 790°C.

Figure 1b Evolution of the ferrite grain size log-normal distribution for the Mo steel at 790°C.

Figure 1c Evolution of the ferrite grain size log-normal distribution for the Mo-Nb-V steel at 800°C.

Figure 2a Increase with time in the number of ferrite grains per unit volume in the plain C steel.

Figure 2b Increase with time in the number of ferrite grains per unit volume in the Mo steel.

Figure 2c Increase with time in the number of ferrite grains per unit volume in the Mo-Nb-V steel.

Figure 3a Nucleation rate versus time in the plain C steel at 820, 800 and 790°C.

Figure 3b Nucleation rate versus time in the Mo steel at 840, 820, 800 and 790°C.

Figure 3c Nucleation rate versus time in the Mo-Nb-V steel at 880, 860, 840, 820 and 800°C.

Figure 4 Dependence of the maximum nucleation rate on temperature in the plain C, Mo and Mo-Nb-V steels.

Figure 5 Evolution of the number of ferrite grains per unit volume for the Mo steel at 800°C under static and dynamic conditions.

Figure 6 Ferrite nucleation rate in the Mo steel at 800°C with different predeformations.

Figure 7a Dependence of the mean grain size of ferrite on growth time in the plain C steel.

Figure 7b Dependence of the mean grain size of ferrite on growth time in the Mo steel.

Figure 7c Dependence of the mean grain size of ferrite on growth time in the Mo-Nb-V steel.

Figure 8 Growth rate parameter α as a function of temperature for the plain C, Mo and Mo-Nb-V steels.

Figure 9 Dependence of the mean grain size of ferrite on growth time at 800°C for different predeformations and strain rates in the Mo steel.

Figure 10 Coherent 'pillbox' nucleus; all interfaces are of low energy. Edge energy $\sigma^{e}_{\alpha\gamma}$. Facet energy within 'upper' austenite grain $\sigma^{c}_{\alpha\gamma}$. Facet energy in grain boundary plane $\sigma^{cb}_{\alpha\gamma}$. Austenite grain boundary energy $\sigma_{\gamma\gamma}$ (10).

Figure 11 Maximum nucleation rates in the plain C, Mo and Mo-Nb-V steels with respect to Ae_3 -T.

Figure 12 Dependence of the growth rate parameter α on the degree of undercooling in the plain C, Mo and Mo-Nb-V steels.

Figure 13 Growth rate parameter α as a function of predeformation for the Mo steel at 800°C.

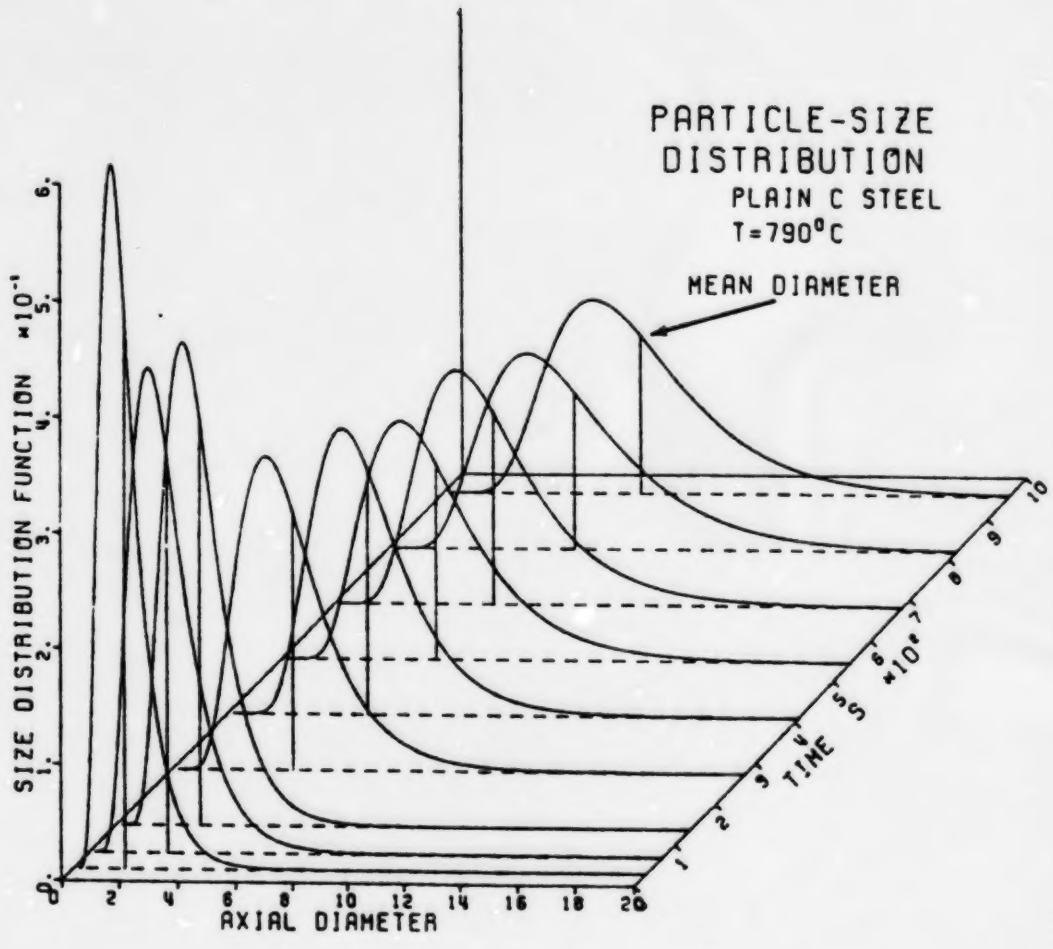

Figure 1a Evolution of the ferrite grain size log-normal distribution for the plain C steel at 790°C.

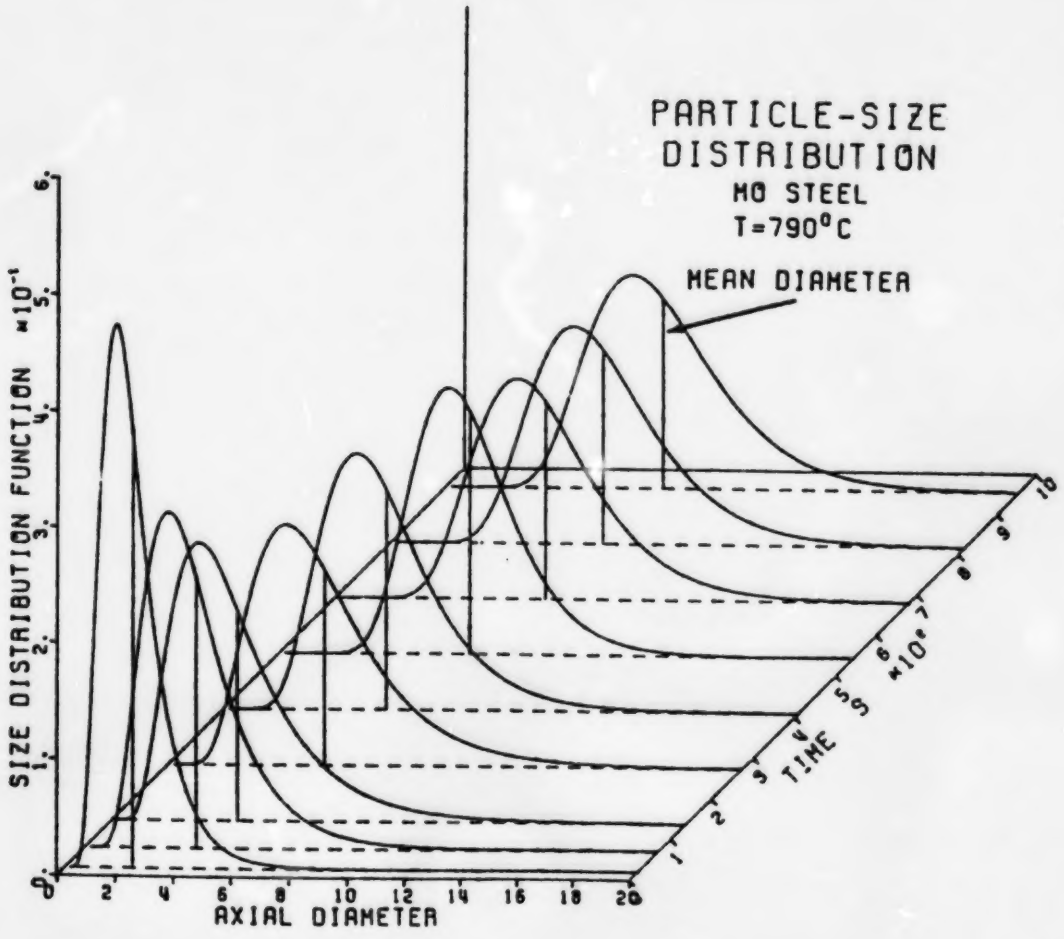

Figure 1b **Evolution of the ferrite grain size log-normal distribution for the Mo steel at 790°C.**

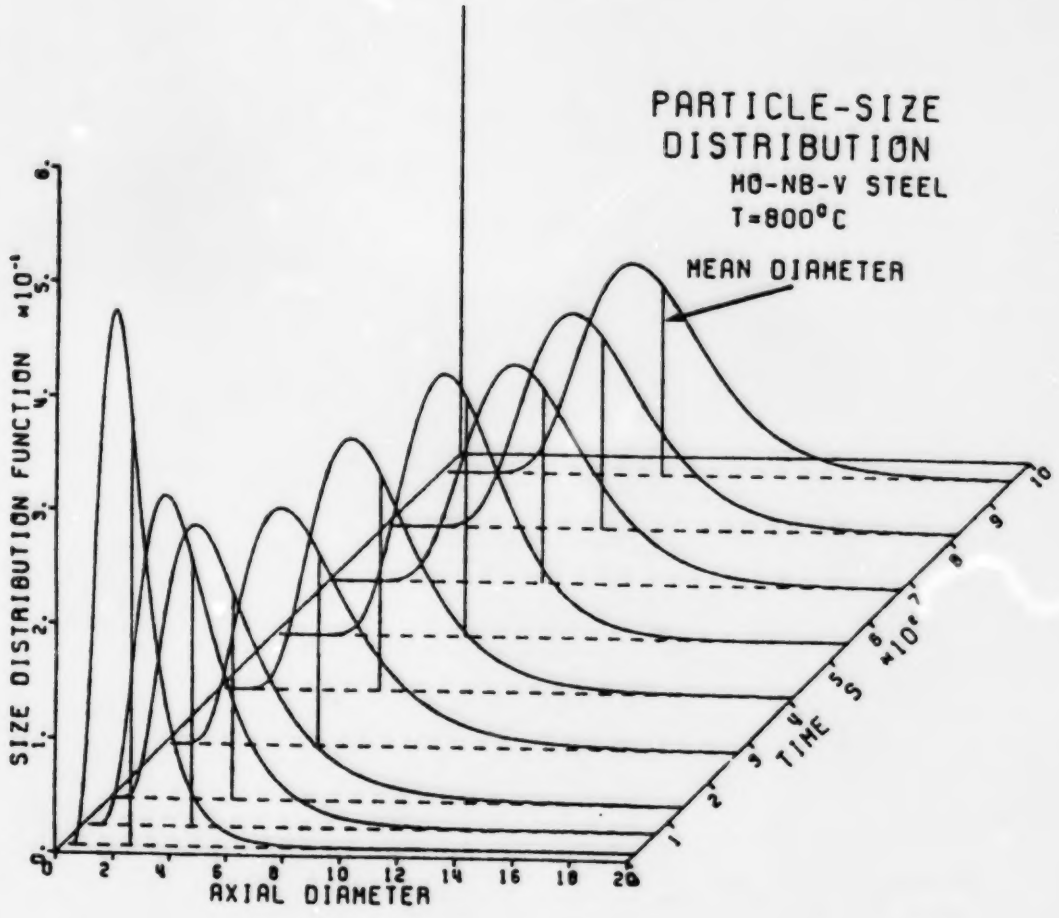

Figure 1c Evolution of the ferrite grain size log-normal distribution for the Mo-Nb-V steel at 800°C.

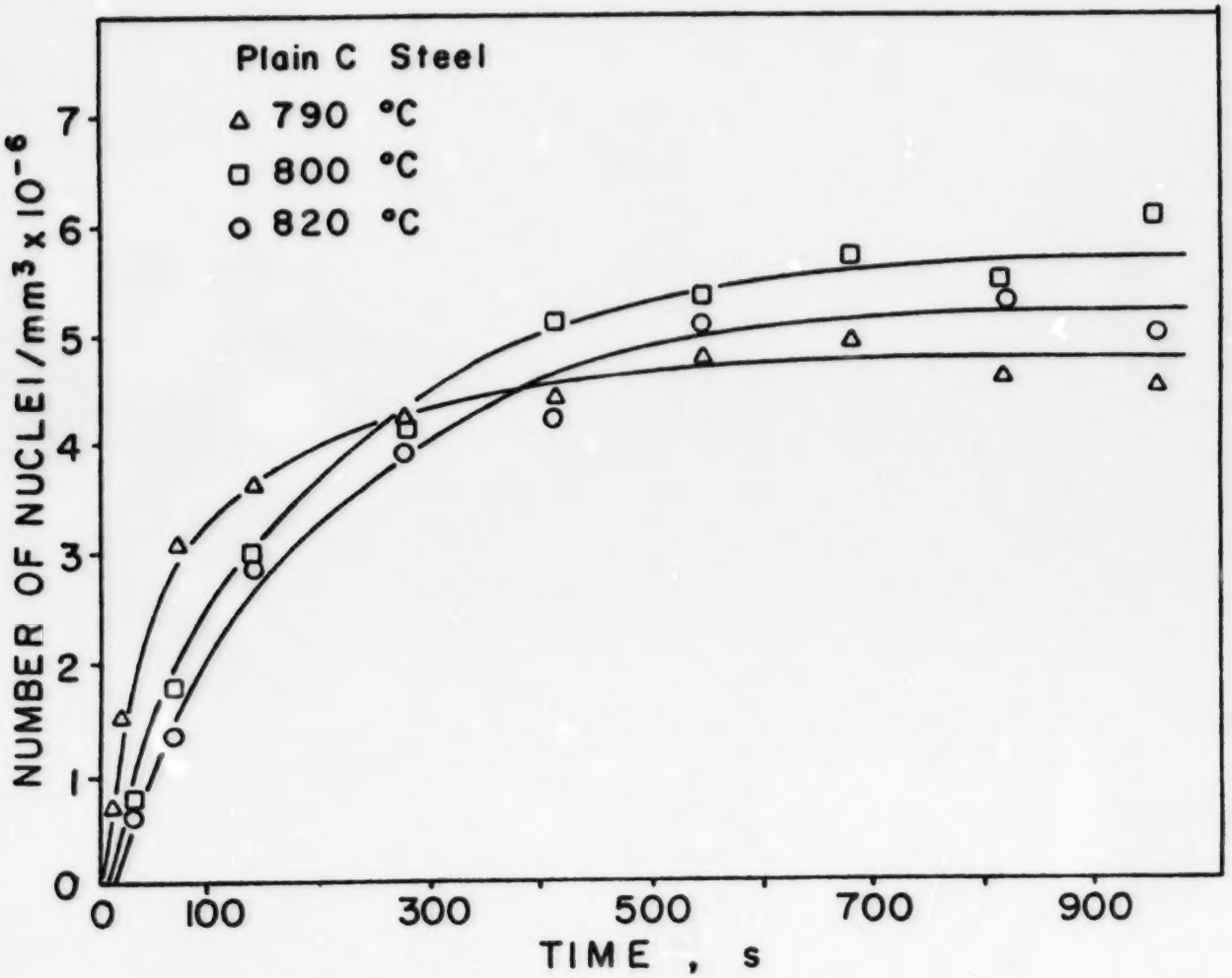

Figure 2a Increase with time in the number of ferrite grains per unit volume in the plain C steel.

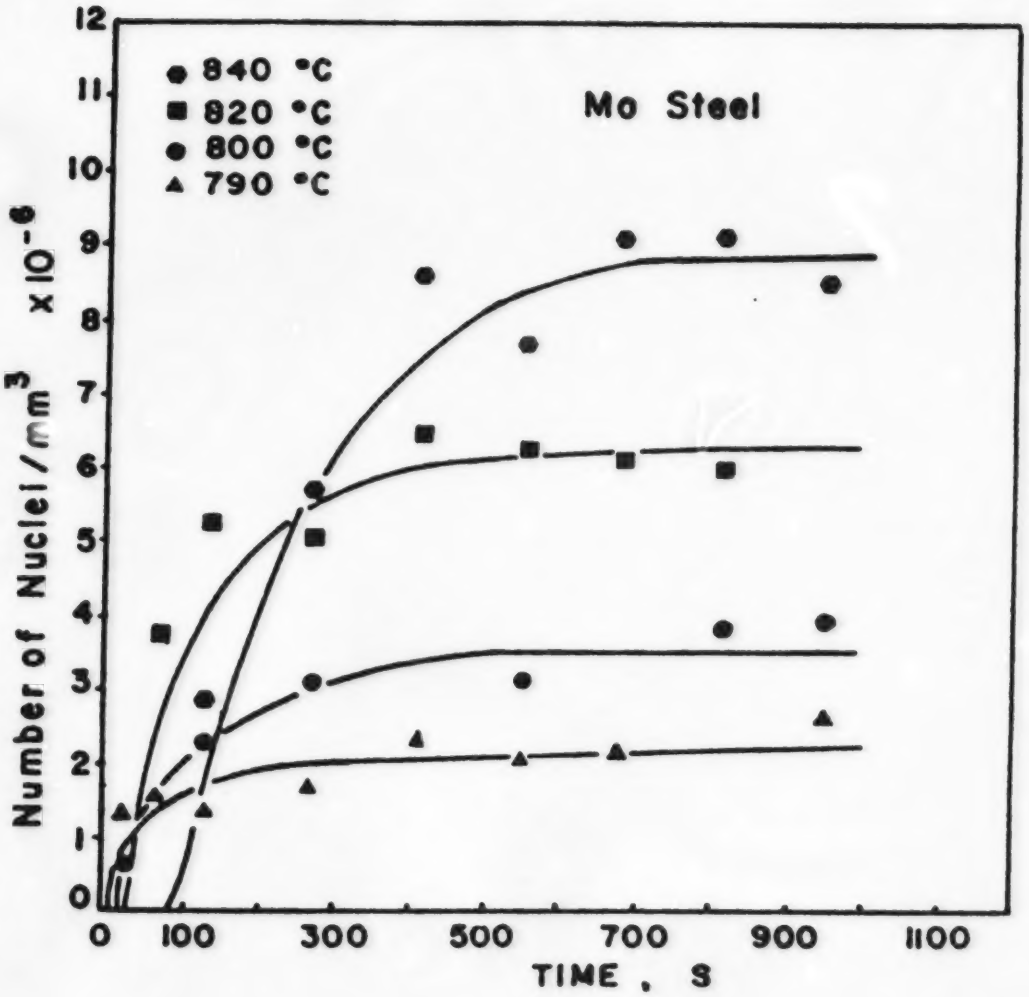

Figure 2b Increase with time in the number of ferrite grains per unit volume in the Mo steel.

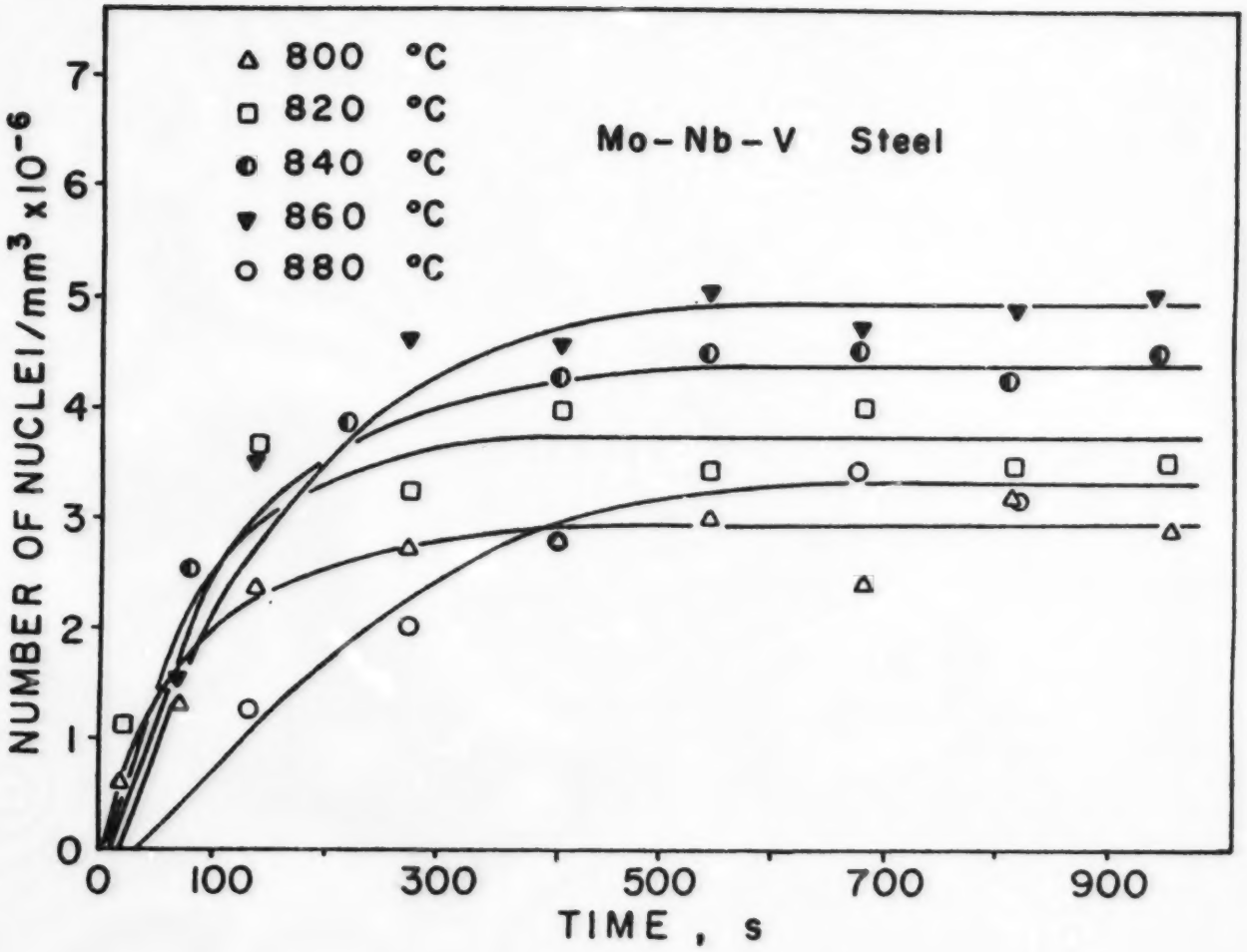

Figure 2c Increase with time in the number of ferrite grains per unit volume in the Mo-Nb-V steel.

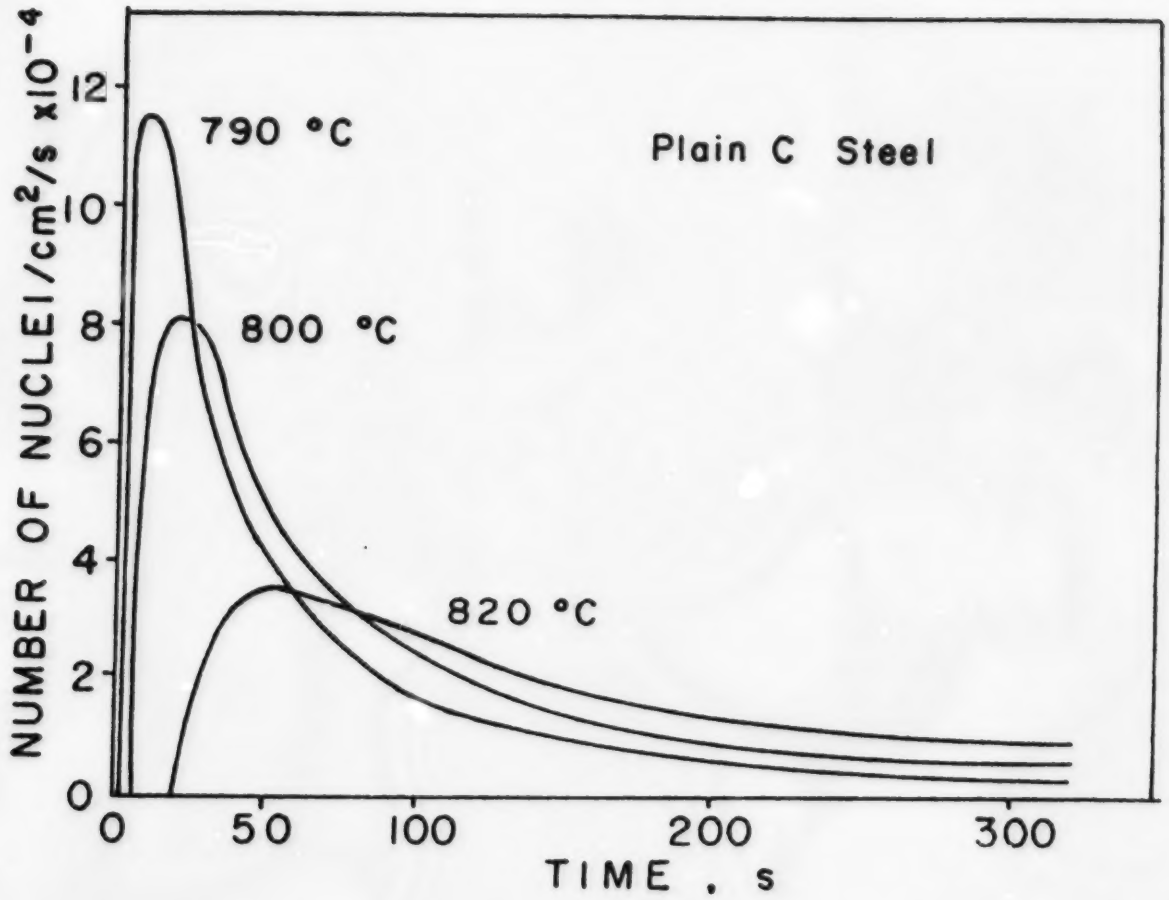

Figure 3a Nucleation rate versus time in the plain C steel at 820, 800 and 790°C.

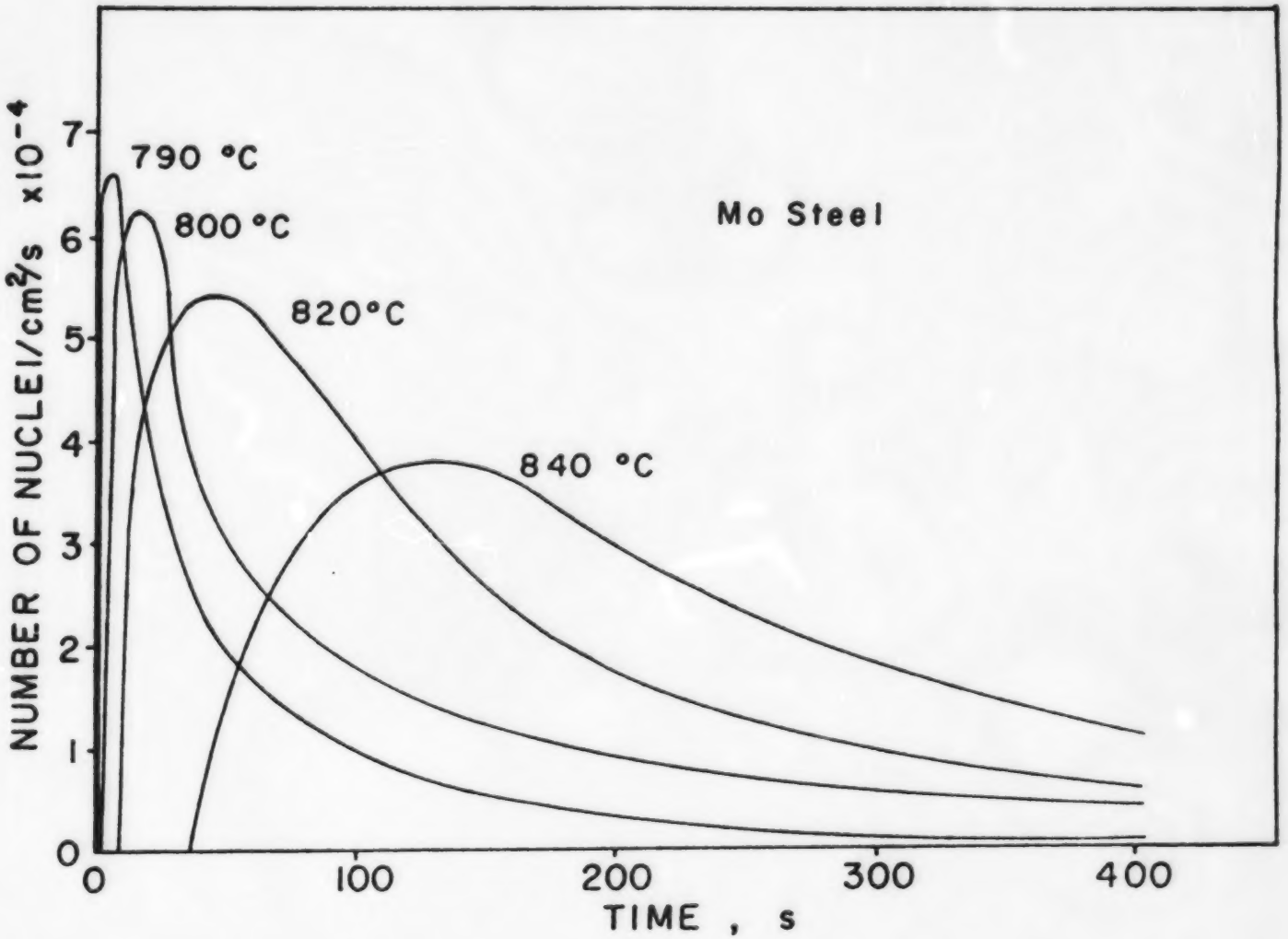

Figure 3b Nucleation rate versus time in the Mo steel at 840, 820, 800 and 790°C.

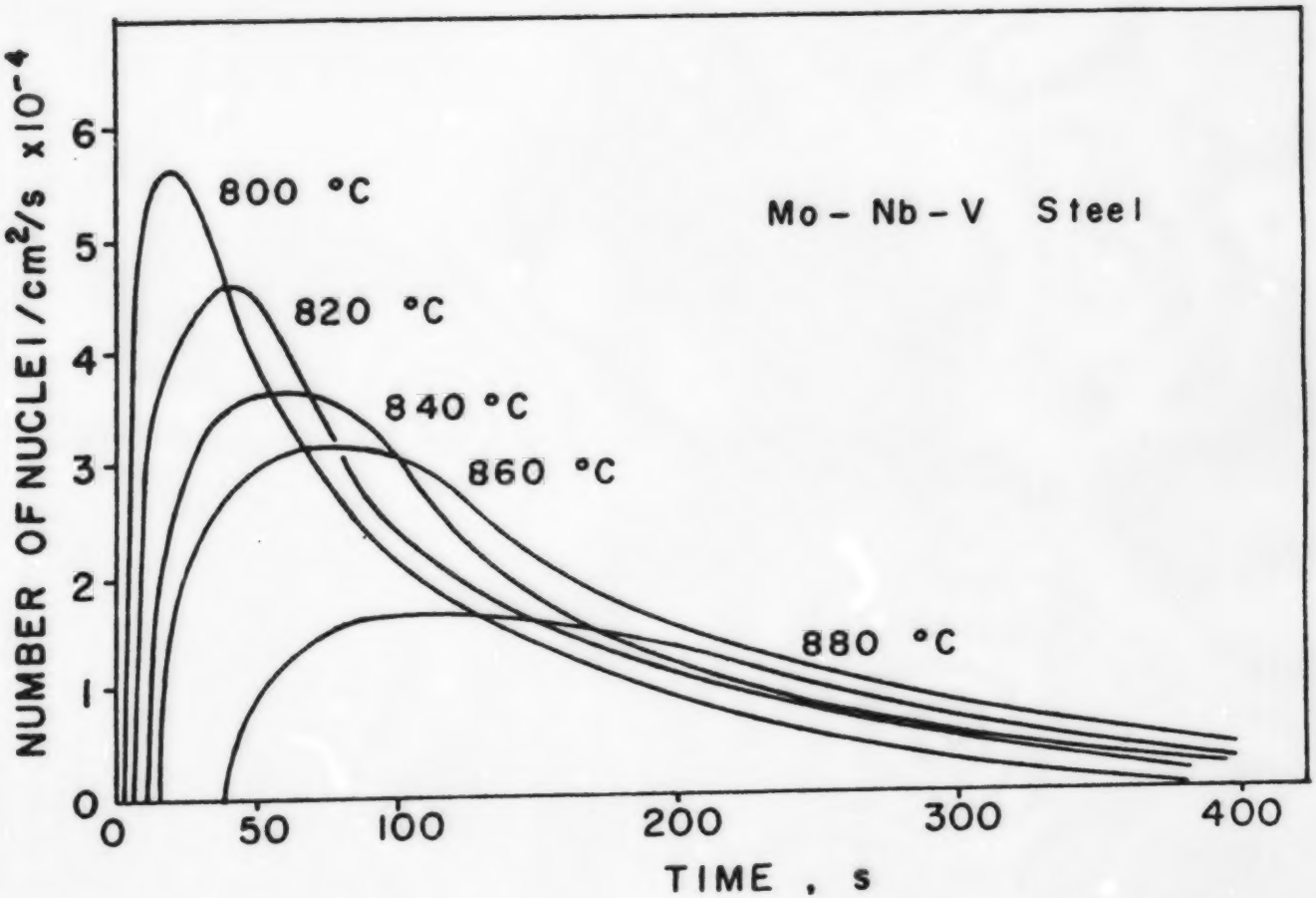

Figure 3c Nucleation rate versus time in the Mo-Nb-V steel at 880, 860, 840, 820 and 800°C.

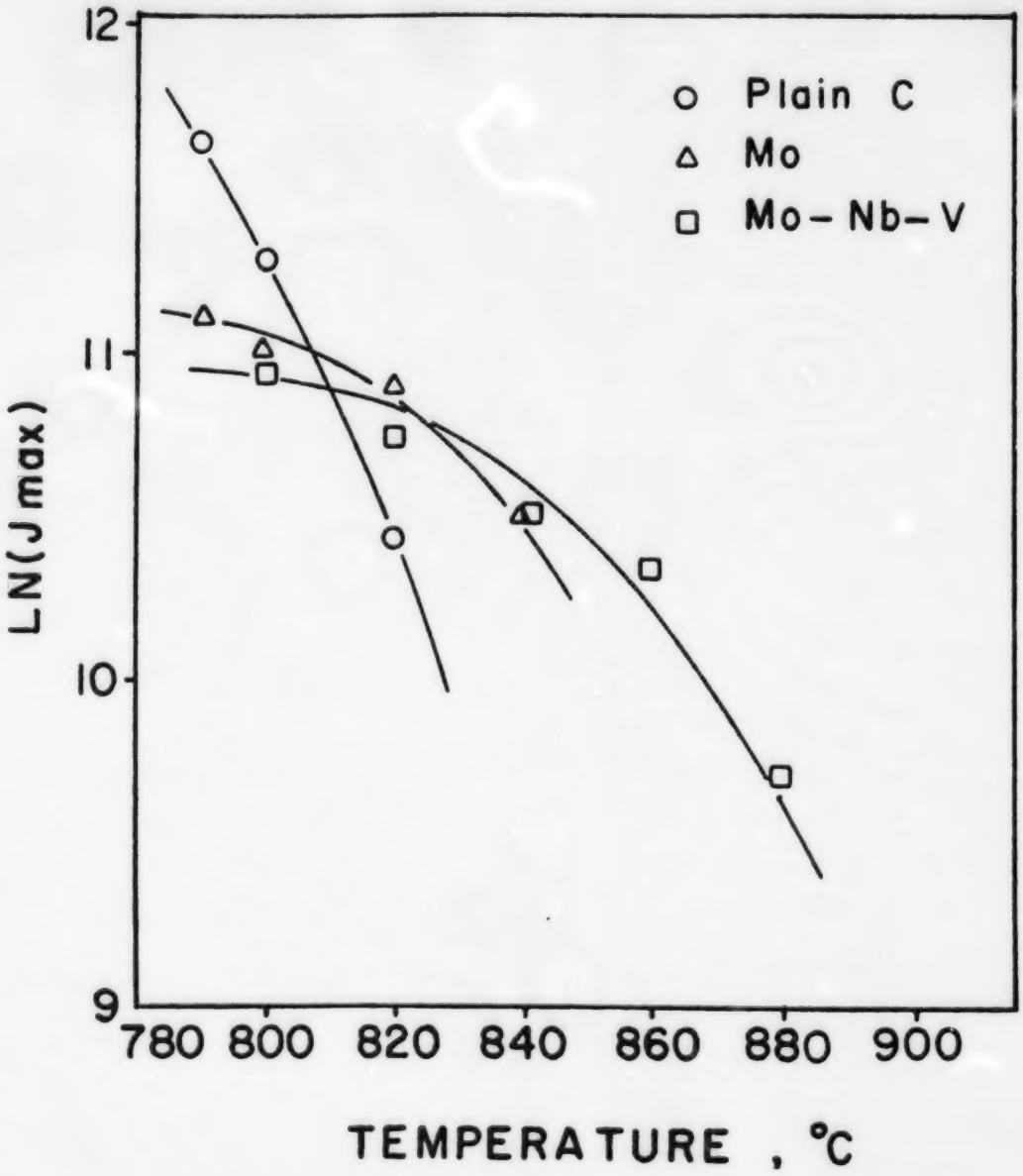

Figure 4 Dependence of the maximum nucleation rate on temperature in the plain C, Mo and Mo-Nb-V steels.

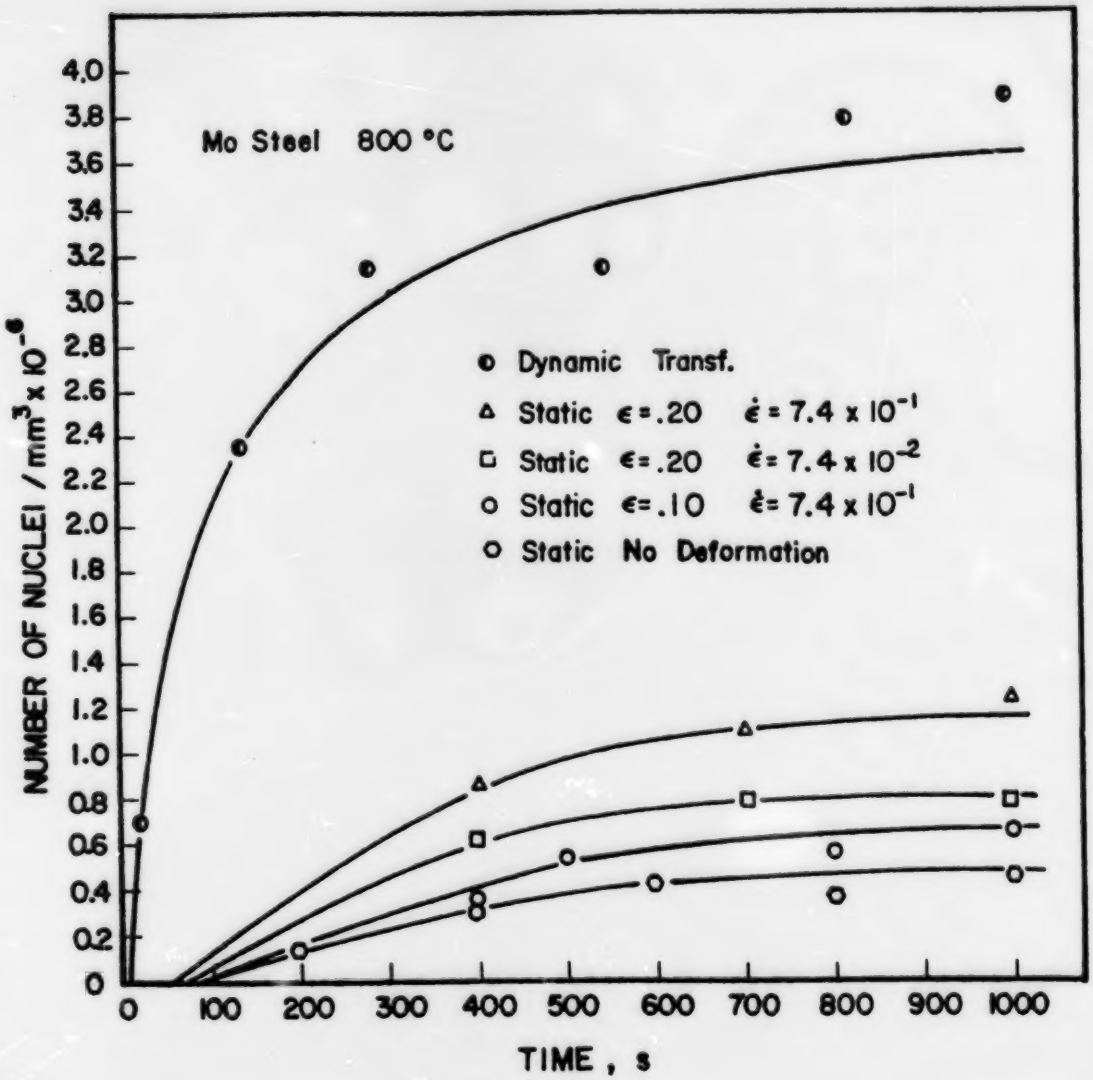

Figure 5 Evolution of the number of ferrite grains per unit volume for the Mo steel at 800°C under static and dynamic conditions.

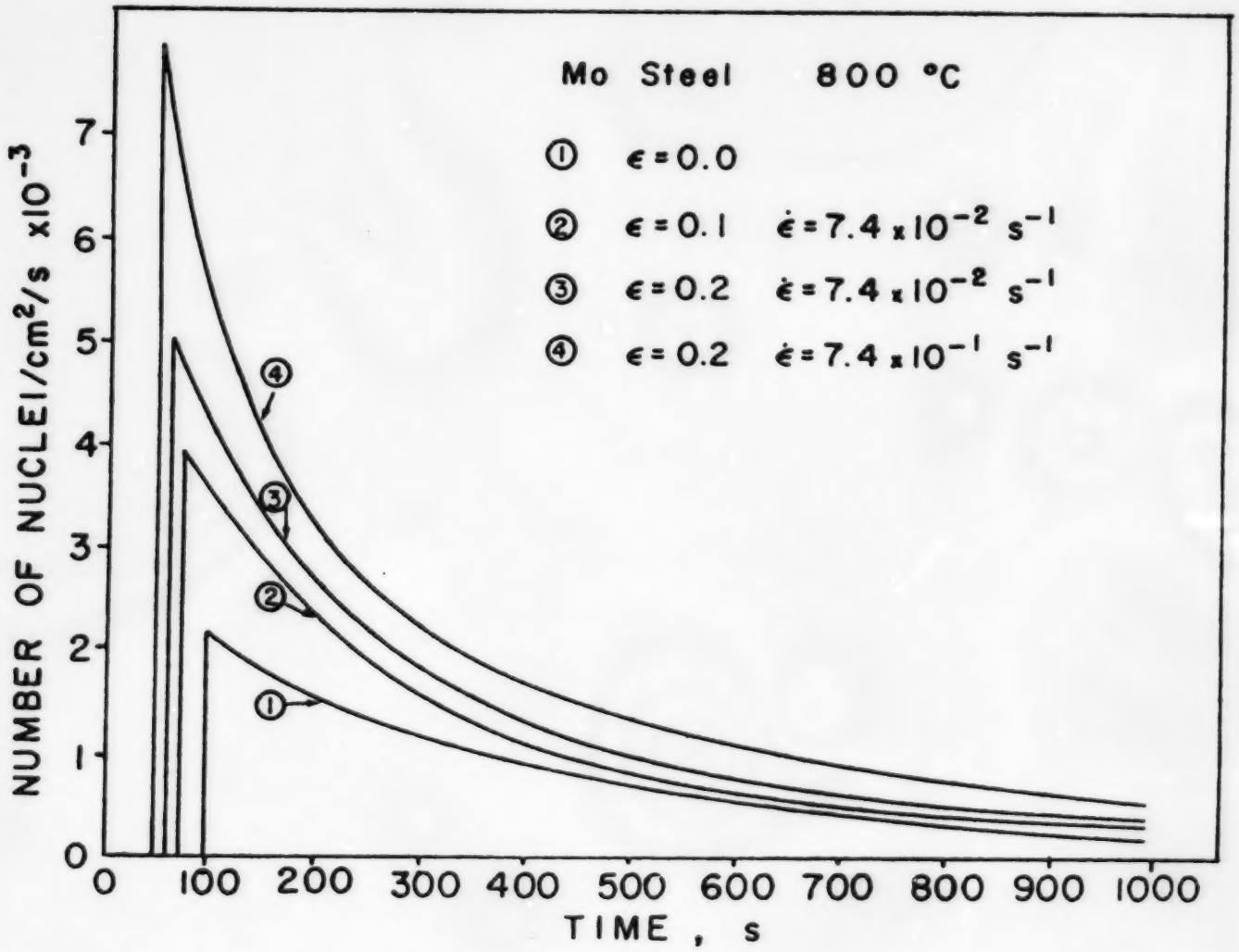

Figure 6 Ferrite nucleation rate in the Mo steel at 800°C with different predeformations.

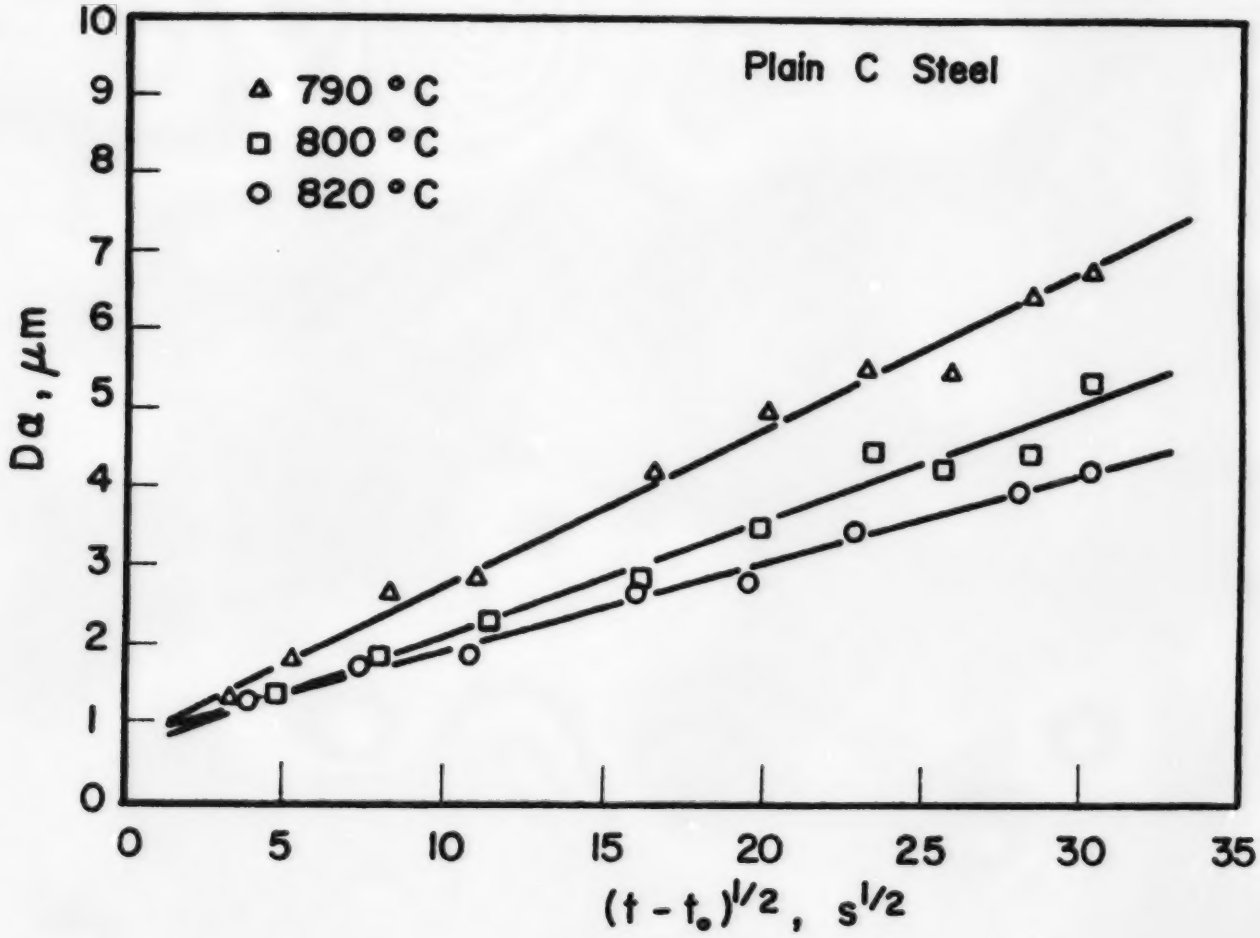

Figure 7a Dependence of the mean grain size of ferrite on growth time in the plain C steel.

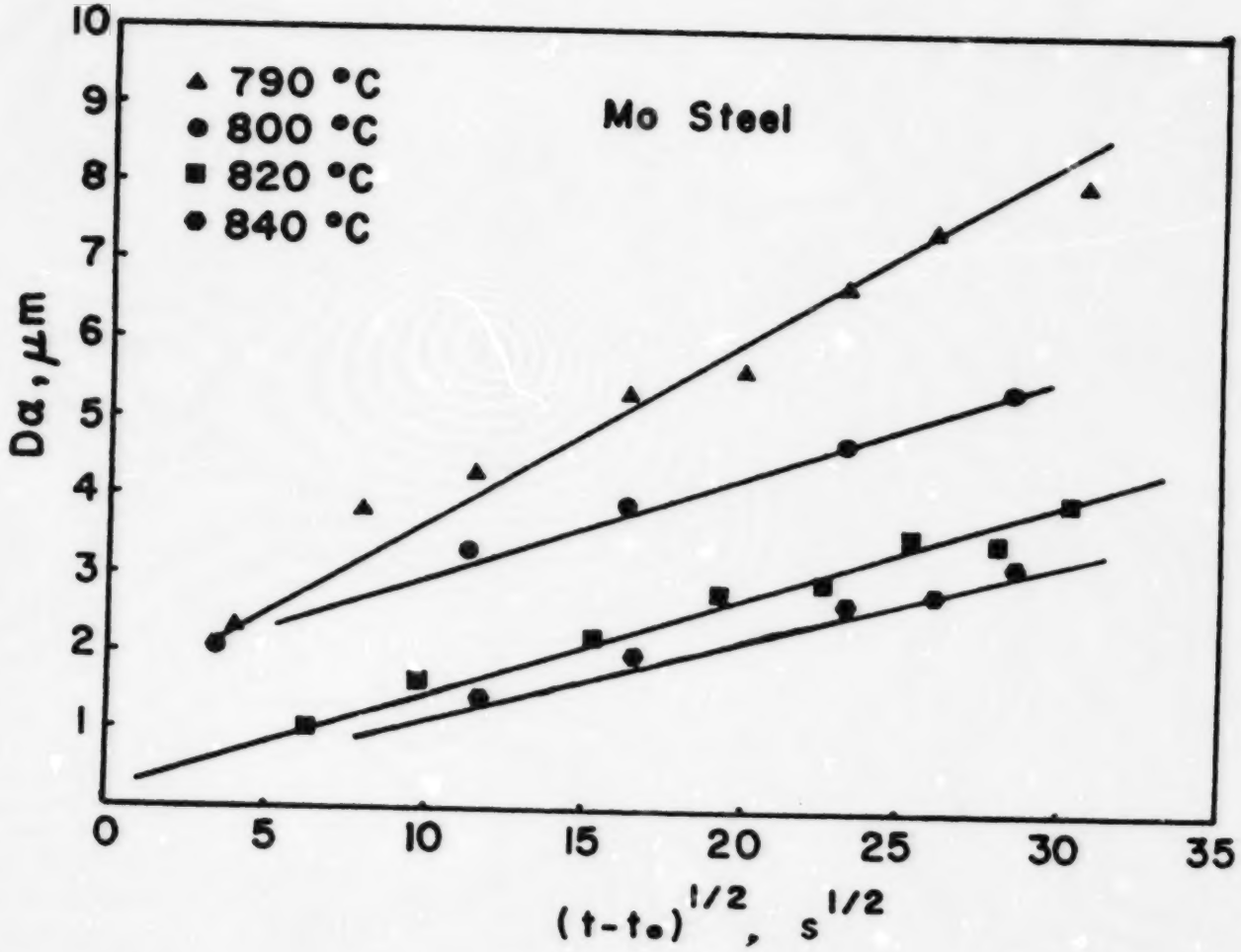

Figure 7b Dependence of the mean grain size of ferrite on growth time in the Mo steel.

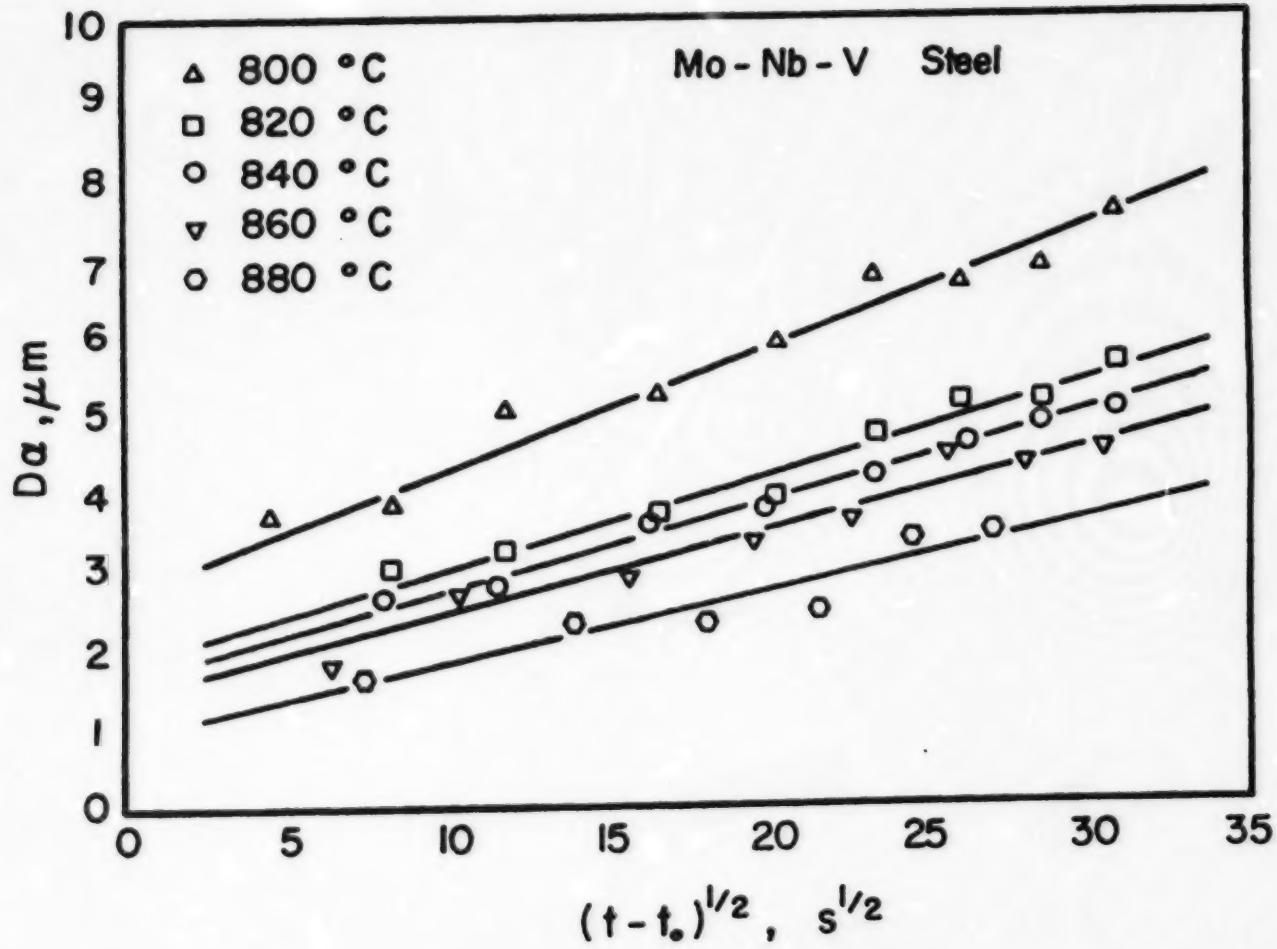

Figure 7c Dependence of the mean grain size of ferrite on growth time in the Mo-Nb-V steel.

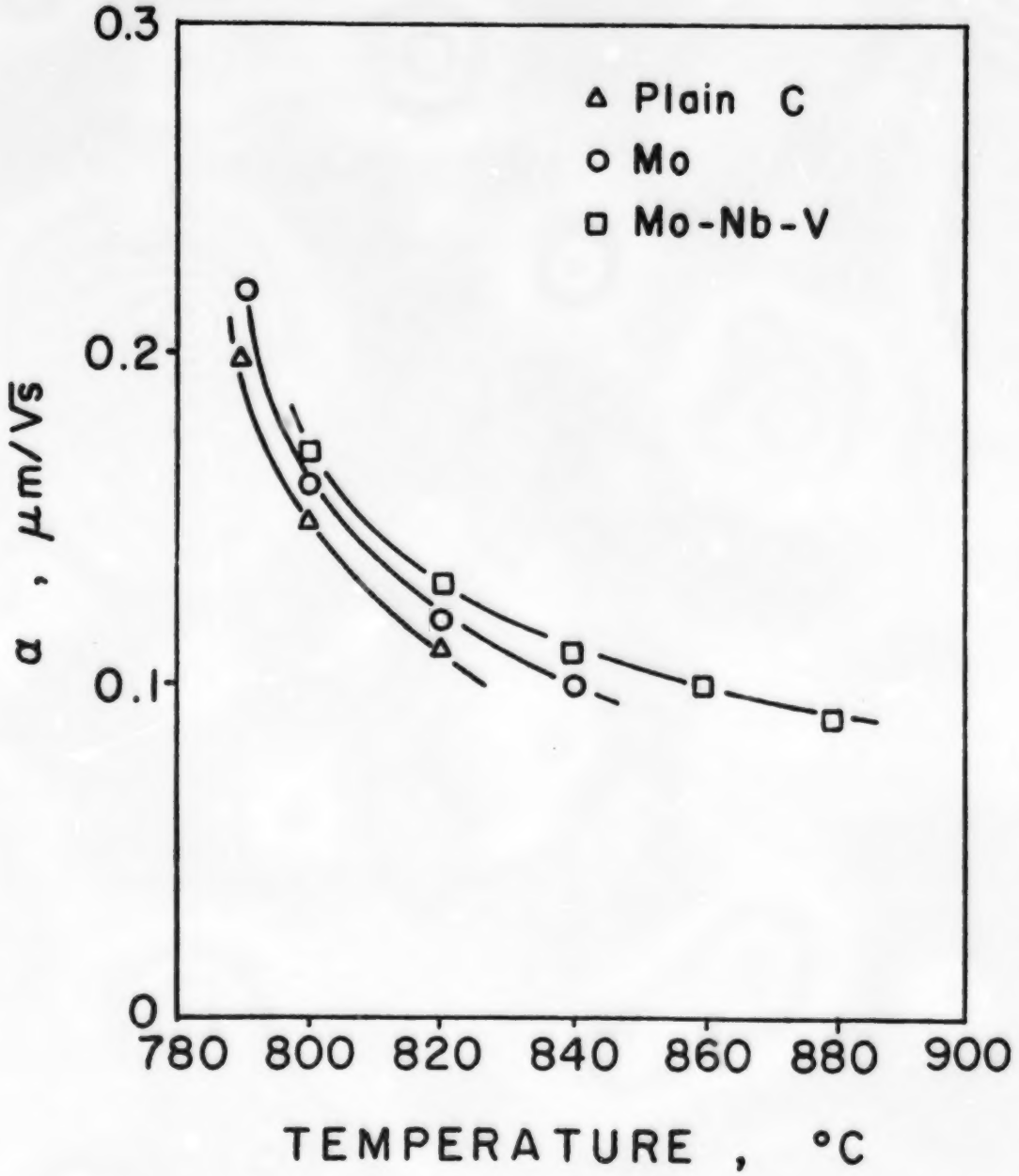

Figure 8 Growth rate parameter α as a function of temperature for the plain C, Mo and Mo-Nb-V steels.

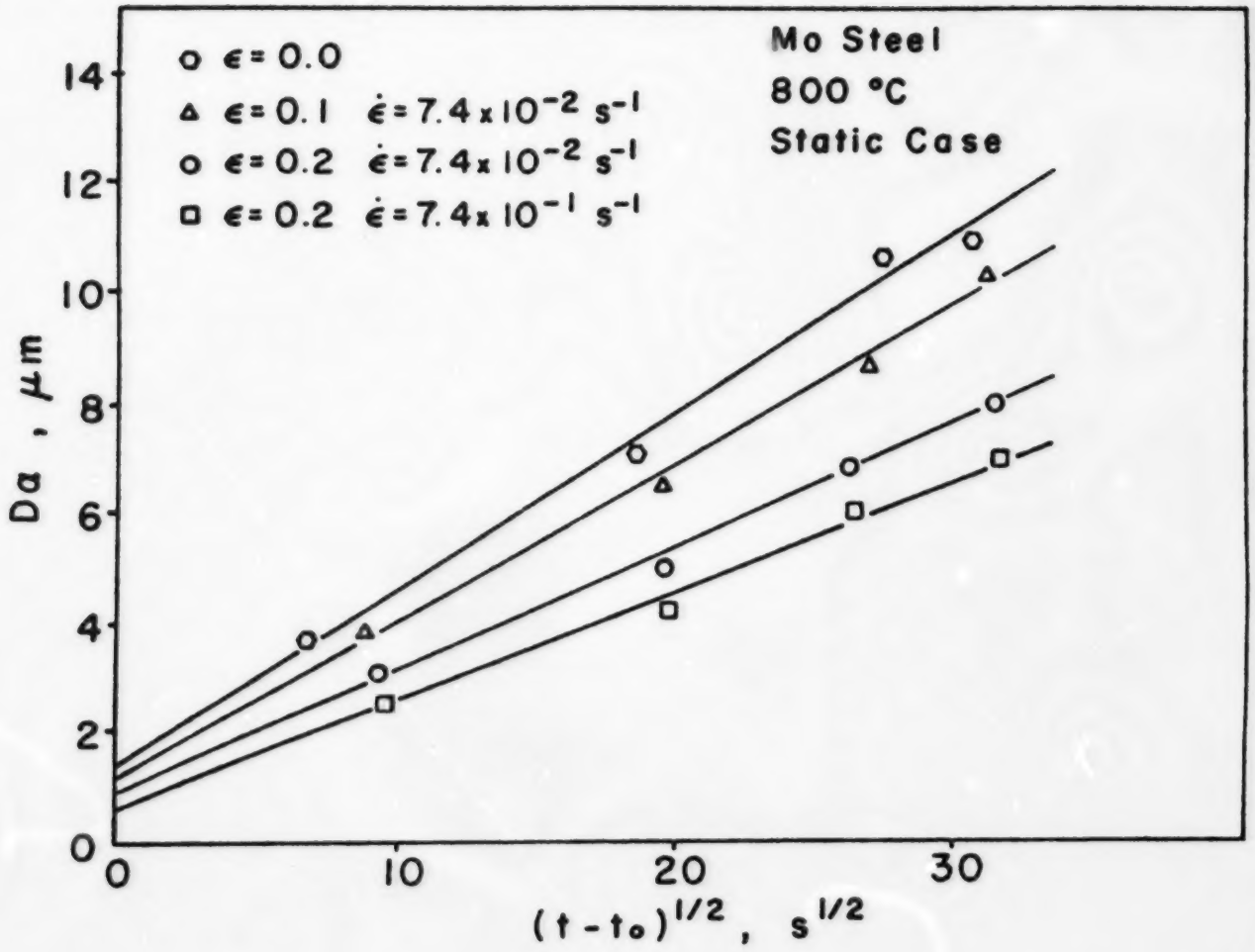

Figure 9 Dependence of the mean grain size of ferrite on growth time at 800°C for different predeformations and strain rates in the Mo steel.

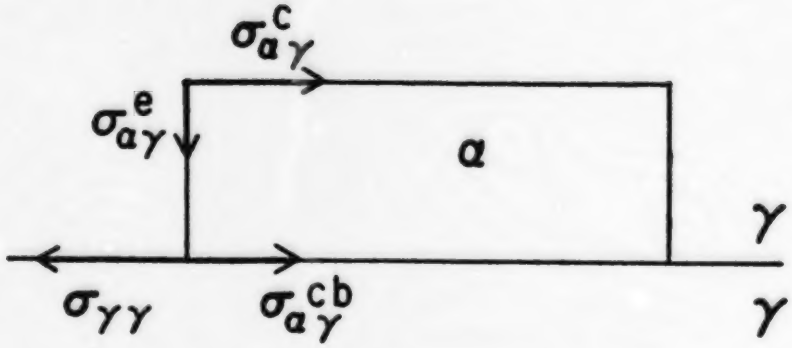

Figure 10 Coherent 'pillbox' nucleus; all interfaces are of low energy. Edge energy $\sigma^{e}_{\alpha\gamma}$. Facet energy within 'upper' austenite grain $\sigma^{c}_{\alpha\gamma}$. Facet energy in grain boundary plane $\sigma^{cb}_{\alpha\gamma}$. Austenite grain boundary energy $\sigma_{\gamma\gamma}$ (10).

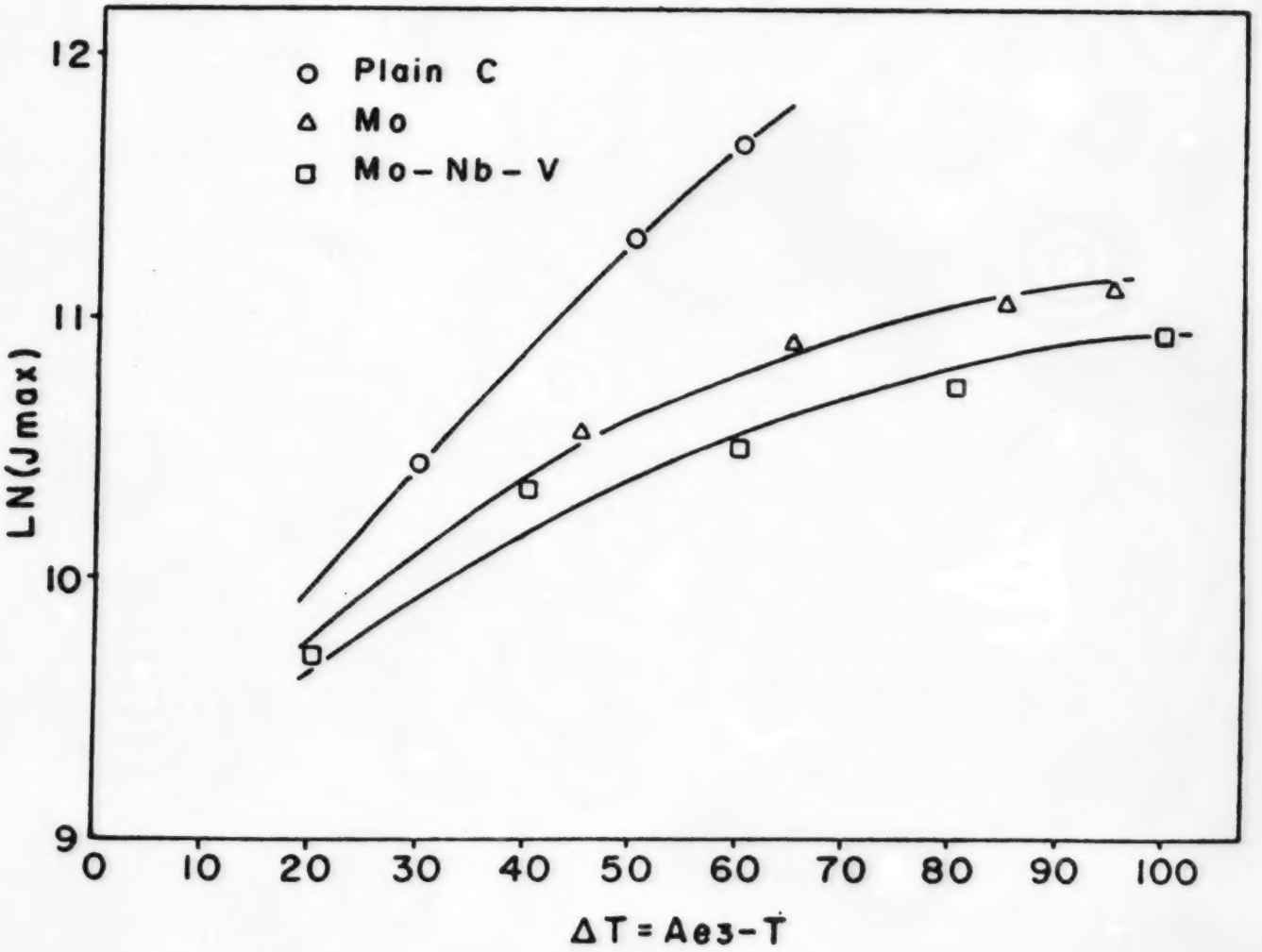

Figure 11 Maximum nucleation rates in the plain C, Mo and Mo-Nb-V steels with respect to Ae_3 -T.

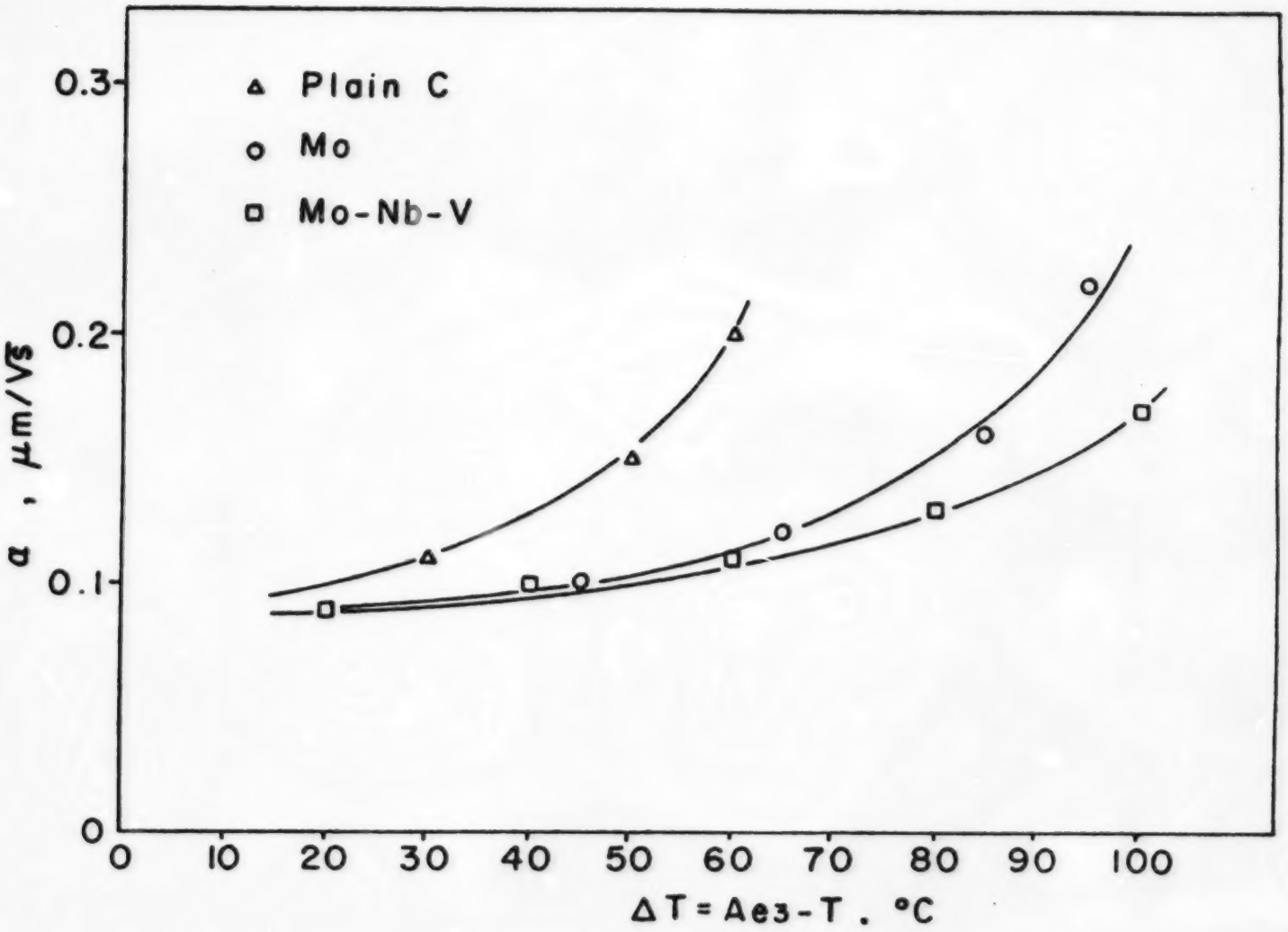

Figure 12 Dependence of the growth rate parameter α on the degree of undercooling in the plain C, Mo and Mo-Nb-V steels.

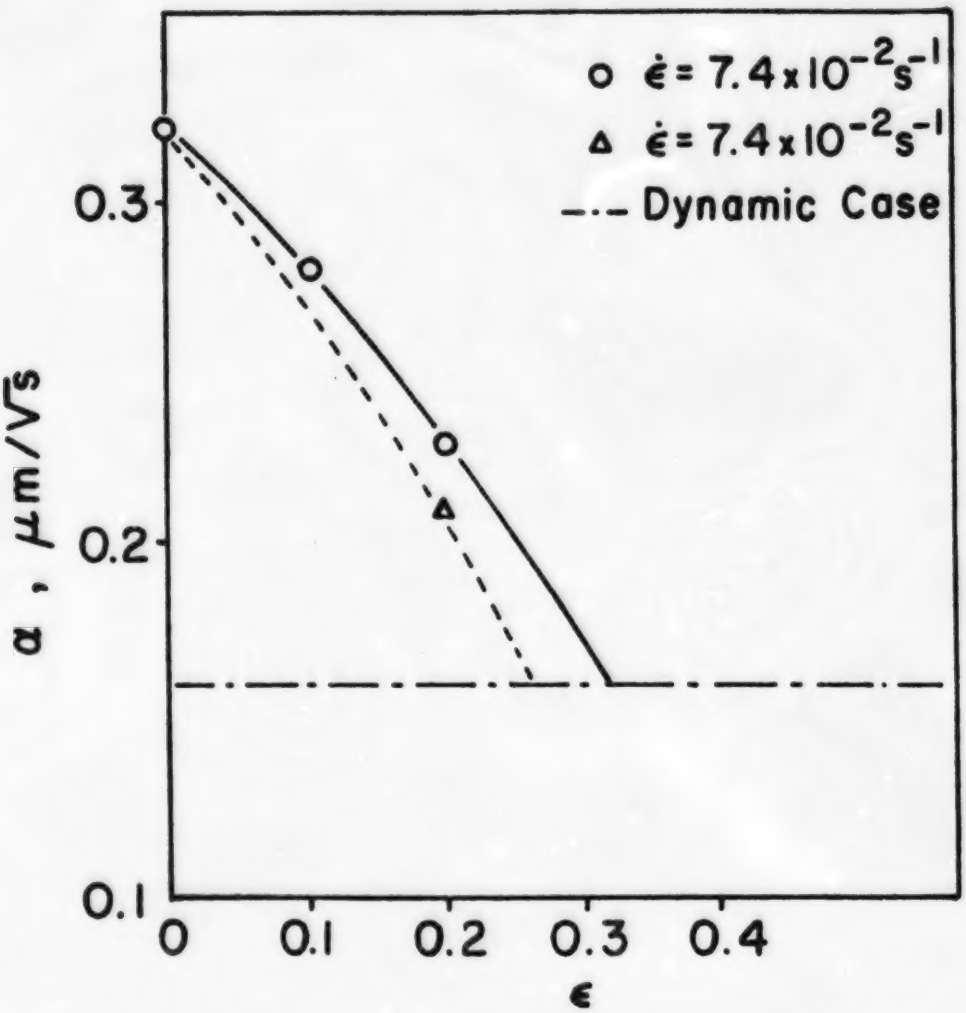

Figure 13 Growth rate parameter α as a function of predeformation for the Mo steel at 800°C.